PNNL-12179
UC-2030

Pacific Northwest
National Laboratory
Operated by Battelle for the
U.S. Department of Energy

Simulation of Hanford Tank 241-C-106 Waste Release into Tank 241-Y-102

Y. Onishi
K. P. Recknagle

May 1999

Prepared for the U.S. Department of Energy
under Contract DE-AC06-76RLO 1830

DISCLAIMER

PACIFIC NORTHWEST NATIONAL LABORATORY
operated by
BATTELLE
for the
UNITED STATES DEPARTMENT OF ENERGY
under Contract DE-AC06-76RLO 1830

Printed in the United States of America

Available to DOE and DOE contractors from the Office of Scientific and Technical Information, P.O. Box 62, Oak Ridge, TN 37831; prices available from (615) 576-8401.

Available to the public from the National Technical Information Service, U.S. Department of Commerce, 5285 Port Royal Rd., Springfield, VA 22161

This document was printed on recycled paper.
(9/97)

PNNL-12179
UC-2030

Simulation of Hanford Tank 241-C-106 Waste Release into Tank 241-AY-102

Y. Onishi
K.P. Recknagle

May 1999

Prepared for
the U.S. Department of Energy
Under Contract DE-AC06-76RLO 1830

Pacific Northwest National Laboratory
Richland, Washington 99352

Executive Summary

Waste stored in Hanford single-shell Tank 241-C-106 will be sluiced with a supernatant liquid from double-shell Tank 241-AY-102 (AY-102) at the U.S. Department of Energy's Hanford Site in Eastern Washington. The resulting slurry, containing up to 30 wt% solids, will then be transferred to Tank AY-102. During the sluicing process, it is important to know the mass of the solids being transferred into AY-102. One of the primary instruments used to measure solids transfer is an Enraf® densitometer located near the periphery of the tank at riser 15S. This study was undertaken to assess how well a densitometer measurement could represent the total mass of solids transferred if a uniform lateral distribution was assumed. The study evaluated the C-106 slurry mixing and accumulation in Tank AY-102 for the following five cases:

Case 1: 3 wt% slurry in 6.4-m AY-102 waste

Case 2: 3 wt% slurry in 4.3-m AY-102 waste

Case 3: 30 wt% slurry in 6.4-m AY-102 waste

Case 4: 30 wt% slurry in 4.3-m AY-102 waste

Case 5: 30 wt% slurry in 5.0-m AY-102 waste.

The time-dependent, three-dimensional, TEMPEST computer code was used to simulate solid deposition and accumulation during the injection of the C-106 slurry into AY-102 through four injection nozzles. The TEMPEST computer code was applied previously to other Hanford tanks, AP-102, SY-102, AZ-101, SY-101, AY-102, and C-106, to model tank waste mixing with rotating pump jets, gas rollover events, waste transfer from one tank to another, and pump-out retrieval of the sluiced waste.

The model results indicate that the solid depth accumulated at the densitometer is within 5% of the average depth accumulation. Thus the reading of the densitometer is expected to represent the total mass of the transferred solids reasonably well.

The AY-102 model predicted that, in all five cases, the C-106 slurry jets descend toward the tank bottom because the heavier C-106 slurry is being injected into the lighter AY-102 supernatant liquid. Predicted solid concentrations for all five cases exhibit significant vertical variation. Of these five cases, Case 2 exhibits the smallest vertical variation of solid loading above the settled solids layer; the finest solid, with 0.1- to 0.5-μm diameters, and the coarsest solid, with 50- to 70-μm diameters, showed about 100% and four orders of magnitude variation, respectively.

In Cases 1 and 2, with only 3 wt% solids, C-106 slurry jets hit the farthest tank wall 2.3 m above the tank bottom. In Cases 3 through 5, with 30 wt% solids, the C-106 slurry jets descend much more rapidly; the plume centers hit the tank bottom and slide along the surface of the original AY-102 sludge layer. Table S.1 shows the predicted dilution of C-106 solids by the time the slurry hits the farthest wall. Note that these values do not represent the settled solids that form after sluicing.

Table S.1. Predicted Dilution of C-106 Solids at the Farthest Tank Wall

	Solids Loading at Injection (kg/m^3)	Solids Loading at Tank Wall (kg/m^3)	Dilution
Case 1	30.34	2.222	13.7
Case 2	30.34	2.269	13.4
Case 3	368.6	21.845	16.9
Case 4	368.6	21.951	16.8
Case 5	366.2	27.451	13.3

Upon hitting the tank wall and bottom, the slurry jet slides along the surface of the original AY-102 sludge layer. The jets injected through four 1-in. nozzles cause the slurry plume to break into four discrete fingers that hit the tank wall and swivel back toward the tank center, exhibiting fan-shaped isoconcentration contours.

Solid deposition patterns vary from case to case and from solid to solid. For example, in Cases 1 and 2, the finer solids accumulate along the tank wall, especially in the four places that the plumes hit, and least around the tank center. The coarser solids accumulate least along the tank wall, except in the area where the four plumes hit the wall, and accumulate most around the tank center. In Cases 3, 4, and 5, with 30 wt% solids, the finer solids accumulate around the four areas the four slurry jets hit and less around the tank center, while the coarser solids accumulate more in the area the reflected jet are moving into.

The horizontal distributions of solid concentrations for all five cases are much more uniform than the vertical distributions. Estimated accumulated depth immediately above the original AY-102 nonconvective layer is shown in Table S.2. This table indicates a relatively small variation of the accumulated depth; e.g., the ratio of the maximum accumulated depth to the average accumulated depth is within 24% for all five cases. The depth at riser 15S, the location of the Enraf densitometer, is expected to be within 5% of the average accumulated depth for all cases.

Table S.2. Estimated Depth Variations of C-106 Solid Accumulation in Tank AY-102

	Ratio of Maximum Depth to Average Depth	Ratio of Average Depth to Depth at Riser 15S	Ratio of Maximum Depth to Depth at Riser 15S
Case 1	1.14	0.970	1.11
Case 2	1.24	1.05	1.30
Case 3	1.09	0.963	1.05
Case 4	1.10	0.976	1.07
Case 5	1.07	0.955	1.02

Contents

Figures

Tables

1.0 Introduction

Tank waste stored in single-shell Tank (SST) 241-C-106 will be sluiced with supernatant liquid from double-shell Tank (DST) 241-AY-102 at the U.S. Department of Energy's Hanford Site in Eastern Washington. The resulting C-106 slurry, containing up to 30 wt% solids, will then be transferred into Tank AY-102. This study evaluates the C-106 slurry mixing and accumulation and determines how uniformly that slurry will be distributed in AY-102 when it is discharged into that tank. During the sluicing process it is important to know the mass of solids transferred into AY-102. One of the primary instruments used to measure solids transfer is an Enraf® densitometer located near the periphery of the tank. This study was undertaken to assess how well a densitometer measurement could represent the total mass of solids transferred if a uniform lateral distribution was assumed.

The diameter and operating height of Tank AY-102 are 23 m (75 ft) and 10.7 m (35 ft), respectively, and its operating storage capacity is 4,300 kL (1,140 kgal). The C-106 slurry will be discharged into AY-102 though four 1-in. injection nozzles oriented at right angles to one another to form a cross in the horizontal plane. They are located 6 ft off tank center and 13 ft above the tank bottom in the study. A 4-in.-suction pipe to recirculate the AY-102 supernatant liquid back to Tank C-106 for continued feed to the sluicing jet is located 22 ft from tank center (28 ft from the slurry inlet distributor) at the surface of the supernatant liquid.

We applied the TEMPEST computer code (Trent and Eyler 1993) to Tank AY-102 to simulate waste jet mixing and solid deposition and accumulation during the injection of the C-106 slurry. The general TEMPEST computer code simulates flow, mass and heat transport, and chemical reactions (equilibrium and kinetic) coupled together (Onishi et al. 1996a). For the fluid mechanics computation, TEMPEST solves three-dimensional, time-dependent equations of flow, turbulence, heat, and mass transport, based on conservation of

- fluid mass (the equation of continuity)
- momentum (the Navier-Stokes equations)
- turbulent kinetic energy and its dissipation
- thermal energy
- mass of dissolved constituents
- mass of solid constituents
- mass of gaseous constituents.

TEMPEST uses integral forms of the fundamental conservation laws applied in the finite volume formulation. It uses the k-ε turbulence model (Rodi 1984) to solve the turbulence kinetic energy and its dissipation. TEMPEST can accommodate non-Newtonian power law fluids as well as fluids whose rheology depends upon solid concentrations (Mahoney and Trent 1995; Onishi and Trent 1998).

The TEMPEST computer code has been applied to Hanford DSTs AP-102 (Onishi and Recknagle 1998), SY-102 (Onishi et al. 1996b), AZ-101 (Onishi and Recknagle 1997), SY-101 (Trent and Michener 1993), and AY-102 (Whyatt et. al. 1996) to model tank waste mixing with

rotating pump jets, gas rollover events, and waste transfer from one tank to another. It was also applied to Tank C-106 to simulate pump-out retrieval of the sluiced waste (Whyatt et. al. 1996).

Section 2 describes the injection-induced mixing conditions, the modeling cases, and their parameters. Section 3 reports model applications and assessment results. The summary and conclusions are presented in Section 4, and cited references are listed in Section 5.

2.0 Selection of Test Cases and Conditions

2.1 Test Cases

It is planned to transfer C-106 sluiced waste slurry, with up to 30 wt% solids, into Tank AY-102 at the rate of 350 gpm. At the early stages of the sluicing operation, the solid concentration in the slurry may be as low as 3 wt% (Carothers et al. 1998). The supernatant liquid level in Tank AY-102 is expected to be 4.3 m for Phase 1 and 6.4 m for the Phase 2 sluicing operation. Previously, the 300 gpm slurry transfer rate was also considered with the AY-102 sludge and supernatant liquid levels of 45 cm and 4.95 m, respectively (Whyatt et al. 1996). We selected the following five cases to evaluate the C-106 slurry jet mixing and solid settling/accumulation in Tank AY-102 to bound the operational conditions:

Case 1: 3 wt% slurry in 6.4-m AY-102 waste. This case represents the 350-gpm release of C-106 slurry with 3 wt% solids in Tank AY-102 in the initial Phase 2 operation (sludge and supernatant liquid thickness of 30 cm and 6.1 m, respectively)

Case 2: 3 wt% slurry in 4.3-m AY-102 waste. This case represents the 350-gpm release of C-106 slurry with 3 wt% solids in Tank AY-102 in the initial Phase 1 operation (sludge and supernatant liquid thickness of 30 cm and 4.0 m, respectively)

Case 3: 30 wt% slurry in 6.4-m AY-102 waste. This case represents the 350-gpm release of C-106 slurry with 30 wt% solids in Tank AY-102 in the Phase 2 operation (sludge and supernatant liquid thickness of 30 cm and 6.1 m, respectively)

Case 4: 30 wt% slurry in 4.3-m AY-102 waste. This case represents the 350-gpm release of C-106 slurry with 30 wt% solids in Tank AY-102 in the Phase 1 operation (sludge and supernatant liquid thickness of 30 cm and 4.0 m, respectively)

Case 5: 30 wt% slurry in 5.0-m Tank AY-102 waste. This case represents the 300-gpm release of C-106 slurry with 30 wt% solids in AY-102 (sludge and supernatant liquid thickness of 45 cm and 4.5 m, respectively).

2.2 Test Conditions

The C-106 slurry will be injected into Tank AY-102 through four 1-in. nozzles, and AY-102 supernatant liquid will be withdrawn through a 4-in. suction pipe. Tank AY-102 contains 1.5 ft of sludge whose bulk density is 1.4 g/mL (Castaing 1994). In the model, we placed the withdrawal suction pipe at 45° between two of the four injection nozzles. To simplify the model and yet maintain some conservatism regarding potential solids settling in the tank, we moved the slurry distributor inlet to the tank center and increased the tank diameter from the actual 75 ft to 81 ft (to account for the 6-ft off-center actual location). This allowed us to simulate the behavior of the jet farthest from the tank wall, and the larger tank volume provided conservatism to the results with respect to heterogeneity of the distributed C-106 slurry.

We assumed that the sluicing operation in Tank C-106 and subsequent pipeline transfer of the C-106 slurry to Tank AY-102 do not change the particle size distribution, so the solids in the C-106 slurry have the same size distribution as the Tank C-106 sludge.

For Cases 1 through 4, we used the solid size distribution with the average particle size of 5 μm, as shown in Table 2.1 (Lumetta et al. 1996). We divided the solids into nine groups (#1 through 9) for the AY-102 modeling. Solid #4 represents the average size of the C-106 solids.

The particle density of the average C-106 solids is 2.28 g/mL; this value was assigned to all nine solid size fractions. The supernatant liquids in Tanks C-106 and AY-102 have densities of 1.17 and 0.99 g/mL, respectively. Unhindered fall velocity was calculated by assuming the fluid viscosity is 0.69 cP, the same as that of pure water at 37°C. Calculated fall velocities and their ratios to the nozzle jet velocity of 10.9 m/s are also shown in Table 2.1. Actual fall velocities will be further reduced by hindering effects due to high solid concentrations, as discussed below.

When solid concentrations are high, particle fall velocity will be reduced from the particle fall velocity under small solid concentration conditions (Vanoni 1975). This reduced (hindered) fall velocity was computed by Equation 2.1 (Perry and Chilton 1973) during the AY-102 simulations.

$$V_s = V_{so}\left\{1 - \frac{C_v}{C_{v\,max}}\right\}^{4.65} \qquad (2.1)$$

Table 2.1. Particle Size Distributions of Tank C-106 Sludge (from Lumetta et al. 1996) Used for Cases 1 through 4

Solid Size	Particle Sizes (μm)	Volume Percent	Unhindered Fall Velocity[(a)] (m/s)	Ratio of Fall Velocity to Jet Velocity
#1	0.1 - 0.5	11.0	5.1×10^{-8}	4.7×10^{-9}
#2	0.5 - 1.0	6.4	5.1×10^{-7}	4.7×10^{-8}
#3	1.0 - 3.0	15.2	3.0×10^{-6}	2.7×10^{-7}
#4	3.0 - 6.0	17.4	1.8×10^{-5}	1.7×10^{-6}
#5	6.0 - 10	15.3	6.1×10^{-5}	5.6×10^{-6}
#6	10 - 20	17.1	2.0×10^{-4}	1.9×10^{-5}
#7	20 - 30	6.2	6.1×10^{-4}	5.6×10^{-5}
#8	30 - 50	6.7	1.5×10^{-3}	1.4×10^{-4}
#9	50 - 75	4.7	3.8×10^{-3}	3.5×10^{-4}
Total		100.0		

(a) Unhindered fall velocity is input to the AY-102 model assuming the fluid is pure water at 37°C.

where

C_V = solid volume fraction of the slurry
C_{vmax} = maximum solid volume fraction
V_S = hindered fall velocity
V_{SO} = unhindered fall velocity (see Table 2.1 for this velocity).

Case 5 used the solid size distribution of C-106 sludge reported by Castaing (1994). Table 2.2 shows this particle size distribution, ranging from 5 to 55 μm, together with associated unhindered fall velocity. The average particle size based on weight is about 16 μm. The density of the all solids was assigned to 2.4 g/mL, as reported by Castaing (1994).

The viscosity of the slurry changes spatially and temporally during the waste transfer operation in Tank AY-102 as a result of mixing the supernatant liquid and solids. The TEMPEST code calculates these varying viscosities during the simulation by Equation 2.2:

$$\mu = \mu_L \left\{ \frac{\mu_s}{\mu_L} \right\}^{\frac{C_v}{C_{v\,max}}} \tag{2.2}$$

where

μ = viscosity of slurry at solid concentration of C_V
μ_L = viscosity of supernatant liquid
μ_s = viscosity of nonconvective layer

Table 2.2. Particle Size Distributions of Tank C-106 Sludge (from Castaing 1994) Used for Case 5

Solid Size	Particle Sizes, (μm)	Volume Percent	Unhindered Fall Velocity[(a)] (m/s)	Ratio of Fall Velocity to Jet Velocity
#1	5 - 10	35	7.6×10^{-5}	8.1×10^{-6}
#2	10 - 15	11	1.9×10^{-4}	2.0×10^{-5}
#3	15 - 20	5	3.6×10^{-4}	3.9×10^{-5}
#4	20 - 25	12	5.8×10^{-4}	6.2×10^{-5}
#5	25 - 35	4.8	8.8×10^{-4}	9.3×10^{-5}
#6	35 - 40	8	1.6×10^{-3}	1.7×10^{-4}
#7	40 - 45	10.8	2.0×10^{-3}	2.1×10^{-4}
#8	45 - 50	7.4	2.5×10^{-3}	2.7×10^{-4}
#9	50 - 55	6	3.1×10^{-3}	3.3×10^{-4}
Total		100.0		

(a) Unhindered fall velocity is input to the AY-102 model assuming the fluid is pure water at 37°C.

Based on Castaing (1994) and previous Hanford tank waste modeling (Trent and Michener 1993; Whyatt et al. 1996), we selected

C_{vmax} = 0.46
μ_L = 0.69 cP
μ_S = 72,500 cP.

The current nonconvective (solid-bearing) layers in Tanks C-106 and AY-102 may exhibit yield stress. However, we assumed that the resulting nonconvective layer in AY-102 would not have yield stress because the waste will be disturbed by 1) sluicing in Tank C-106, 2) transfer through the 3-in. pipeline connecting the tanks, and 3) injection and deposition of the mixed slurry in Tank AY-102.

3.0 AY-102 Model Results

3.1 Case 1: 3 wt% Slurry in 6.4-m AY-102 Waste

Case 1 represents the 350-gpm-release of C-106 slurry with 3 wt% solids in Tank AY-102 and sludge and supernatant thicknesses of 30 cm and 6.1 m. Thus it corresponds to the first stage of C-106 transfer under the Phase 2 operation (Carothers et al. 1998). The test results for case 1, as explained by the following text, estimated the maximum accumulated depth is 11% more than the depth measured at riser 15S, where the Enraf densitometer is located.

Solid concentrations in the C-106 slurry with 3 wt% solid at injection nozzles are shown in Table 3.1. The densities of the slurry containing 3 wt% C-106 solids are expected to be 1.010 g/mL, so a slightly heavier slurry will be discharged into the lighter AY-102 supernatant liquid of density 0.99 g/mL.

Table 3.1. Solid Concentrations in kg/m^3 at Injection Nozzles, Cases 1 and 2

Solid	#1	#2	#3	#4	#5	#6	#7	#8	#9
Concentration (kg/m^3)	3.34	1.94	4.58	5.22	4.64	5.25	1.91	2.03	1.43

If a negatively buoyant slurry with approximately 10 wt% or more solid materials is released into water, and the ratio of the solid fall velocity to jet (exit) velocity at the release point is less than 0.05, the solid materials behave as a part of a negatively buoyant plume rather than individual solids settling toward the bottom (Brandsma and Sauer 1983). Because the C-106 slurry in this case has only 3 wt% solids, and the ratio of the unhindered fall velocity of C-106 solids to nozzle jet velocity is between $7x10^{-9}$ and $3.5x10^{-4}$ (see Table 2.1), the solids, even larger solids, are not expected to settle down separately from the rest of the slurry plume.

Figure 3.1 shows the predicted vertical distributions of Solid #1 (0.1–0.5-μm-diameter solids) concentration after three simulation minutes. It shows the initial 30-cm-thick nonconvective layer at the tank bottom and the 6.08-m-thick convective (supernatant liquid) layer, totaling 6.38 m of the waste in Tank AN-102. It also shows the position of one of the nozzles injecting a 10.9-ft/s jet within the convective layer. The Solid #1 concentration within the nonconvective (solid bearing) layer is 68.42 kg/m^3, as shown in the figure. Its concentration in the convective layer was initially assigned a small value (0.1 kg/m^3) to handle the fall velocity of the solid for all solid concentrations.

This figure also shows the time (three simulation minutes) at its top and a constituent (Solid #1) near the injection nozzle. The left side of the figure describes the plane it is showing (in this case the r-z plane, which is vertical plane 9 at the 3 o'clock position [I=9]), on the plot (in this case J=1 to 27, indicating the entire radial direction from tank center to wall, and K=1 to 29, indicating the vertical direction from tank bottom to the waste surface at 6.38 m). The right side of the figure also shows concentrations (in kg/m^3) represented by lines 1 through 15. Plane min

and max indicate minimum and maximum values (Solid #1 concentrations of 0.09938 and 68.42 kg/m^3, respectively, in this case) within the plotted plane, while array min and max indicate minimum and maximum values (Solid #1 concentrations of 0.09938 and 68.42 kg/ m^3, respectively, in this case) encountered within the entire simulated volume. At the bottom right, the maximum velocity encountered in this vertical plane is shown (8.432 m/) with its corresponding scale length. All velocity in the plot is scaled to this magnitude. Note that the jet velocity at the nozzle exit is 10.9 m/s in this simulated case. The maximum velocity of 8.432 m/s in this figure is the velocity just outside the nozzle, not at the nozzle exit.

Figure 3.1 shows the slurry plume gradually descending from one of the four nozzles toward the tank bottom. The plume center hits the farthest corner near the bottom. Since the initial concentration of Solid #1 is 3.34 kg/m^3 at the nozzle injection point, this figure shows very rapid mixing at the beginning. The slurry density current then spreads over the original 30-cm-deep AY-102 sludge layer, mixing little with the original tank sludge. Near the surface of the tank, in the supernatant liquid, there is very little Solid #1 at this very early time. Figures 3.2 and 3.3 show the predicted concentrations of Solid #4 (3.0–6.0-μm-diameter) and Solid #9 (50–75-μm-diameter) on the same vertical plane. The Solid #4 settling pattern is similar to that of Solid #1. Although the C-106 slurry descends as a negative plume, some of the coarsest solids are separating from the rest of the plume, as shown in Figure 3.3 depicting Solid #9 settling more quickly to the bottom than others due to its greater fall velocity.

Corresponding solid distributions after one simulation hour are shown in Figures 3.4 through 3.6 for Solids #1, 4 and 9, respectively. Overall patterns of rapidly descending solids are similar to those at three simulation minutes. The slurry plume hits the farthest wall 2.3 m above the tank bottom (or 1.65 m below the injection level) at approximately 0.070 m/s, 155 times less than the injection velocity of 10.9 m/s.

All solids except #9 show somewhat higher concentrations, including those within the descending plume at one simulation hour, than those at three simulation minutes, because the solids with very small fall velocities are floating (see Figures 3.4 and 3.5). However, as shown in Figure 3.6, Solid #9, with the largest fall velocity, settled on the surface of the original AY-102 nonconvective layer more quickly. This rapid descent reduces solid concentrations in the supernatant liquid layer, including those within the plume. There are significant vertical variations of solid concentrations, but horizontal variations of solid concentrations at a given depth become more uniform as the injection time becomes longer. This is especially true for the finer solids, which display less vertical variation below the injection nozzle at one simulation hour.

Near the farthest tank wall, where the plume hits, the initial slurry is diluted by a factor of 13.7. The coarser solids show more dilution, possibly because some of these solids have fallen from the plume. Dilution of each solid at the farthest tank wall 2.3 m above the tank bottom is shown in Table 3.2. The calculated slurry density at this location is 0.9940 g/mL compared with 0.9936 g/mL 6.4 m above the bottom (the surface of the original supernatant liquid) after one simulation hour. Because the jet density (0.9947 g/mL) is no longer greater than that of the waste immediately below, 7.7 m from the injection nozzle and 3.2 m above the bottom, the jet hitting the wall is no longer negatively buoyant but has a neutrally buoyant momentum with a velocity of 0.07 m/s.

Table 3.2. Predicted Reduction of C-106 Solids at the Farthest Tank Wall, Case 1 after 1 hr of Slurry Transfer

Solid	Solids Loading at Injection (kg/m^3)	Solids Loading at Tank Wall (kg/m^3)	Reduction Factor
Solid #1	3.34	0.286	11.7
Solid #2	1.94	0.208	9.3
Solid #3	4.58	0.361	12.7
Solid #4	5.22	0.391	13.4
Solid #5	4.64	0.358	13.0
Solid #6	5.25	0.363	14.5
Solid #7	1.19	0.157	12.2
Solid #8	2.03	0.076	26.7
Solid #9	1.43	0.021	67.1
Total	30.34	2.222	13.7

The diluted C-106 slurry jet slides along the surface of the original AY-102 sludge layer when it hits the tank wall and bottom. The injection jets cause the slurry plume to break into four discrete fingers that hit the tank wall and swivel back toward tank center, producing fan-shaped iso-concentration contours. Finer solids and coarser solids display significantly different deposition patterns.

The finer solid deposition pattern is shown in Figures 3.7 and 3.8, depicting predicted Solid #1 concentrations on a horizontal plane just above the original AY-102 sludge layer after three simulation minutes and one simulation hour, respectively. These figures show that the solids accumulate along the tank wall, especially in the four places that the plumes hit, and that tank center accumulates the least amount of solids. A similar solid deposition pattern was produced by Solid #4, as shown in Figure 3.9 at one simulation hour.

As shown in Figure 3.10, Solid #9 accumulated least along the tank wall, except around the area where the four plumes hit, and most around the tank center. This pattern again reflects the effects of the larger fall velocity on solid settling and slurry flows after the plumes impinge the tank wall and move on the surface of the original AY-102 nonconvective layer.

We examined the variation of the solid accumulation pattern and the adequacy of using a single depth measurement with the Enraf densitometer at riser 15S to represent the average solid accumulation depth. Riser 15S is 11 m (37 ft) from the injection nozzles and 22° from one of the nozzle injection directions. We estimated this by examining the predicted solid concentrations just above the original AY-102 nonconvective layer (30 cm above tank bottom) at the end of one simulation hour. As shown in Table 3.3, the estimated maximum accumulated depth is 14% more than the average accumulated depth, which, in turn, is 3% less than the depth accumulated at riser 15S. Thus, the maximum depth would be 11% greater than the depth at riser 15S, indicating the degree of accuracy the Enraf densitometer provides in representing the average tank accumulation.

Table 3.3. Estimated Depth Variation of C-106 Solid Accumulation in Tank AY-102, Case 1, after 1 hr of Slurry Transfer

Maximum Solid Volume Fraction	Solid Volume Fraction at Riser 15S	Average Solid Volume Fraction	Ratio of Maximum Depth to Average Depth	Ratio of Average Depth to Depth at Riser 15S	Ratio of Maximum Depth to Depth at Riser 15S
0.00965	0.00870	0.00844	1.14	0.970	1.11

The AY-102 model predicted that solids deposited on the original AY-102 nonconvective layer, producing a significant vertical concentration variation within the convective layer. However, the finer solids tend to be more uniformly distributed, because they recirculate upward to compensate for the downward plume movement, and to flow toward the suction pipe that is withdrawing 350 gpm at the supernatant liquid surface.

3.2 Case 2: 3 wt% Slurry in 4.3-m AY-102 Waste

Case 2 modeling conditions were identical to those of Case 1 except that the AY-102 supernatant liquid thickness was assumed to be 4.0 m, reflecting the Stage 1 operating condition (Carothers et al. 1998). The test results for case 2, as explained by the following text, estimated the maximum accumulated depth is 30% more than the depth measured at riser 15S.

The predicted velocity and Solid #1 concentration in a vertical plane containing one of the four nozzles at three simulation minutes and one simulation hour are shown in Figures 3.11 and 3.12, respectively. Both figures show descending patterns for the Solid #1 plume with the plume centers hitting the tank wall. Similar patterns for Solids #4 and 9 are shown in Figures 3.13 and 3.14, respectively.

The slurry plume in this case also hits the farthest tank wall about 2.3 m above the tank bottom. However, its speed near the wall in this case is only 0.033 m/s, 326 times less than the injection velocity of 10.9 m/s. Thus the plume velocity in Case 2 is much less than in Case 1.

The vertical variation in solid concentration in this case is less than in Case 1. For example, Solid #1 shows approximately 100% higher concentration just above the settled solids layer than near the surface. Solid #9 displays about four orders of magnitude variation vertically. Within the depth below the injection nozzle (3.95 m above tank bottom), Solids #1 and 9 display vertical variations of 80% and three orders of magnitude, respectively. As in Case 1, the horizontal variation of solid concentration at a given depth becomes much more uniform. This is especially true for the finer solids.

The jet density (0.9947 g/mL) is no longer higher than that of the waste immediately below, 9.3 m from the injection nozzle and 3.2 m from the bottom. Hence the jet hitting the tank wall is no longer negatively buoyant jet but is a neutrally buoyant momentum jet. Near the farthest wall, where the plume hits, the initial slurry is diluted by a factor of 13.4, similar to the 13.7

value in Case 1. Like Case 1, the coarser solids show more dilution. Dilution of each solid at the farthest tank wall, 2.3 m above the tank bottom, is shown in Table 3.4. The calculated slurry density at this location is 0.9946 g/mL, very similar to the 0.9942 g/mL 4.3 m above the tank bottom (the surface of the original supernatant liquid) after one simulation hour.

When it reaches the AY-102 sludge, the C-106 plume slides on the AY-102 sludge surface, as shown in Figures 3.15 through 3.17 for Solids #1, 4, and 9. Similar to Case 1, Solids #1 and 4 accumulate most around the tank wall and least around tank center, the opposite of the Solid #9 pattern.

Using the predicted solid concentrations just above the original AY-102 nonconvective layer (30 cm above tank bottom) at the end of one simulation hour, we estimated the variation of solids accumulation, as shown in Table 3.5. This case has more varying depths than Case 1. The estimated maximum accumulated depth in Case 2 is 24% more than the average accumulated depth, which, in turn, is 5% less than the depth accumulated at riser 15S, implying that the Enraf densitometer reading represents the average tank solids accumulation conditions very well. The maximum depth would be 30% greater than the depth at riser 15S in this case.

Table 3.4. Predicted Reduction of C-106 Solids at the Farthest Tank Wall, Case 2 after 1 hr of Slurry Transfer

Solid	Solids Loading at Injection kg/ m^3	Solids Loading at Tank wall kg/ m^3	Reduction Factor
Solid #1	3.34	0.302	110
Solid #2	1.94	0.214	9.0
Solid #3	4.58	0.377	12.1
Solid #4	5.22	0.414	12.6
Solid #5	4.64	0.368	12.6
Solid #6	5.25	0.371	14.1
Solid #7	1.19	0.137	14.0
Solid #8	2.03	0.068	30.0
Solid #9	1.43	0.017	82.8
Total	30.34	2.269	13.4

Table 3.5. Predicted Depth Variation of C-106 Solid Accumulation in Tank AY-102 after 1 hr of Slurry Transfer

Maximum Solid Volume Fraction	Solid Volume Fraction at Riser 15S	Average Solid Volume Fraction	Ratio of Maximum Depth to Average Depth	Ratio of Average Depth to Depth at Riser 15S	Ratio of Maximum Depth to Depth at Riser 15S
0.00923	0.00710	0.00746	1.24	1.05	1.30

3.3 Case 3: 30 wt% Slurry in 6.4-m AY-102 Waste

Case 3 represents the 350-gpm-release of C-106 slurry, with 30 wt% solids in AY-102 and sludge and supernatant liquid thicknesses of 30 cm and 6.1 m, respectively. It corresponds to the Phase-2 C-106 transfer condition (Carothers et al. 1998). The Case 3 modeling conditions are identical to those of Case 1 except that it contains 30 wt% solids. The C-106 slurry, with 1.195 g/mL density, is injected into the AY-102 supernatant liquid with 0.990 g/mL density. Thus a significantly heavier slurry will be discharged into the lighter AY-102 supernatant liquid. The test results for case 3, as explained by the following text, estimated the maximum accumulated depth is 5% greater than the depth measured at riser 15S. Solid concentrations in the C-106 slurry, with 30 wt% solids, at injection are shown in Table 3.6 for Cases 3 and 4. The particle size distribution is the same as Case 1, as shown in Table 2.1.

Table 3.6. Solid Concentrations in kg/m^3 at Injection Nozzles, Cases 3 and 4

Solid	#1	#2	#3	#4	#5	#6	#7	#8	#9
Concen-tration (kg/m^3)	39.4	22.9	54.1	61.5	54.7	61.9	22.5	24.0	16.7

Because the ratio of the solid fall velocity to jet (exit) velocity at the injection point is much smaller than 0.05 (see Table 2.1), and solid concentrations are above 10 wt%, the C-106 slurry in Case 3 behaves as if it were one heavy fluid rather than individual solids settling to the bottom. Thus, although C-106 solids are chemically and physically complex, their overall behavior (slurry mixing and deposition during the release to AY-102) is expected to be similar to that of dredged sediments in surface waters (e.g., rivers, estuaries, and coastal waters) (Brandsma and Divoky 1976) and of drilling mud in coastal waters (Runchal 1983).

Predicted velocity and concentration of Solids #1 and 9 in a vertical plane containing one of the four nozzles at one simulation hour are shown in Figures 3.18 and 3.19, respectively. These figures show that Solids #1 and 9 have almost identical distribution patterns and that the slurry jet descends very rapidly, with the plume centers hitting the tank bottom. The slurry plume in this case is diluted such that by the time it is 4.3 m from the injection nozzle and 3.17 m above the bottom, the density of the plume (1.007 g/mL) is the same as that just below the jet; thus it loses its negative buoyancy. However, because of its momentum inertia, the jet plume keeps descending toward the bottom until it is 5.2 m from the injection nozzle and 0.84 m above the tank bottom. At that location, the diluted jet center velocity becomes 0.21 m/s. The jet then starts to spread horizontally, and, subsequently, its center starts to move slightly upward, hitting the farthest tank wall 2.7 m above the tank bottom. Near this wall, the jet velocity is approximately 0.04 m/s and the density is 1.006 g/mL. The velocity reduction here is 270 times the initial injection velocity of 10.9 m/s, much more reduction than in Cases 1 and 2.

The vertical variation of solid concentration in this case is similar to Case 1; for example, Solid #1 displays its concentrations above the settled layer, showing an approximately 30-fold vertical variation. Within the depth below the injection nozzle (3.95 m above bottom), Solids #1

and 9 display vertical variations of two-fold and many orders of magnitude, respectively. Like Case 1, horizontal variation of the solid concentration at a given depth is much less.

Near the farthest tank wall, where the plume eventually hits, the initial slurry is diluted by a factor of 16.9—more than the 13.7 in Case 1. As in Case 1, the coarser solids show more dilution. Dilution of each solid at the farthest tank wall, 2.7 m above the bottom, is shown in Table 3.7. The calculated slurry density of 1.006 kg/m^3 at this location is still much higher than the 0.9936 g/mL 6.4 m above the bottom (the surface of the original supernatant liquid) after one hour. This density difference makes it difficult for the slurry to move upward.

Upon descending to the AY-102 sludge surface, the C-106 plume slides horizontally to deposit many of the solids it is carrying. This is shown in Figures 3.20 and 3.21 for Solids #1 and 9 just above the AY-102 sludge surface. These figures show that the finer solids accumulate more around the four areas the slurry jets hit and less around the tank center; the coarser solids accumulate more in the area the reflected slurry is moving into, including regions between the location of the original slurry jet pass and the tank center.

The estimated variation of the solid accumulation in this case is shown in Table 3.8. This case has less depth variation than Case 1. The estimated maximum accumulated depth for Case 3 is 9% more than the average, which, in turn, is 3.7% less than the depth accumulated at riser 15S. revealing the degree of accuracy the Enraf densitometer can provide. The maximum depth would be 5% greater than the depth at riser 15S in this case.

Table 3.7. Predicted Reduction of C-106 Solids at the Farthest Tank Wall in Case 3 after 1 hr of Slurry Transfer

Solid	Solids Loading at Injection kg/ m^3	Solids Loading at Tank Wall kg/ m^3	Reduction Factor
Solid #1	39.4	2.69	14.7
Solid #2	22.9	1.59	14.4
Solid #3	54.1	3.64	14.9
Solid #4	61.5	4.12	15.0
Solid #5	54.7	3.62	15.1
Solid #6	61.9	3.92	15.8
Solid #7	22.5	1.25	18.0
Solid #8	24.0	0.82	29.4
Solid #9	16.7	0.21	80.3
Total	368.6	21.85	16.9

Table 3.8. Estimated Depth Variation of C-106 Solid Accumulation in Tank AY-102, Case 3 after 1 hr of Slurry Transfer

Maximum Solid Volume Fraction	Solid Volume Fraction at Riser 15S	Average Solid Volume Fraction	Ratio of Maximum Depth to Average Depth	Ratio of Average Depth to Depth at Riser 15S	Ratio of Maximum Depth to Depth at Riser 15S
0.0417	0.0398	0.0383	1.09	0.963	1.05

3.4 Case 4: 30 wt% Slurry in 4.3-m AY-102 Waste

Case 4 represents the 350-gpm release of C-106 slurry into AY-102 with 30 wt% solids and sludge and supernatant liquid thickness of 30 cm and 4.0 m, respectively. It corresponds to the Phase 1 C-106 transfer condition (Carothers et al. 1998). Thus the Case 4 modeling conditions are identical to those of Case 2 except that the C-106 slurry contains 30 wt% solids. Solid concentrations in the C-106 slurry at the injection nozzles in Case 4 are shown in Table 3.6. The particle size distribution is the same as Cases 1 through 3, as shown in Table 2.1. The test results for case 4, as explained by the following text, estimated the maximum accumulated depth is 7% greater than the depth measured at riser 15S. As in Case 3, the C-106 slurry in Case 4 behaves as one heavy fluid rather than individual solids settling to the tank bottom, because the ratio of the solid fall velocity to jet (exit) velocity at the release point is much smaller than 0.05 (see Table 2.1), and solid concentrations are above 10 wt%.

The solid distribution pattern in this case was expected to be similar to that of Case 3. Calculated velocity and concentrations of Solids #1 and 9 in the vertical plane containing one of the four nozzles at one simulation hour are shown in Figures 3.22 and 3.23, respectively. These figures show that Solids #1 and 9 descend very rapidly, with the plume centers hitting the tank bottom. The slurry plume in this case is diluted such that by the time it is 3.4 m away from the injection nozzle and 3.4 m above the tank bottom, its density (1.009 g/mL) is the same as that just below the jet; it has lost its negative buoyancy. The jet plume keeps descending toward the bottom. When it is 5.2 m away from the injection nozzle and 0.84 m above the tank bottom, the diluted jet center velocity becomes 0.21 m/s. The jet then starts to spread horizontally, and its center starts to go slightly upward, hitting the farthest tank wall 2.3 m above tank bottom. Near this wall, the jet velocity is approximately 0.05 m/s and the density is 1.006 g/mL. The velocity is 220 times less than the initial injection velocity, 10.9 m/s.

The vertical variation of solid concentration for this case is still large, as in Case 3. For example, Solid #1 displays its concentrations above the settled solid layer with approximately four-fold vertical variation. Within the depth below the injection nozzle (3.95 m above tank bottom), Solids #1 and 9 display vertical variations of two-fold and many orders of magnitude, respectively. Horizontal variations of the solid concentrations at a given depth are much smaller.

Near the farthest tank wall, where the plume eventually hits, the initial slurry has been diluted by a factor of 16.8, which is almost identical to that of Case 3 and greater than the 13.4 dilution of Case 2. Dilution of each solid at the farthest tank wall 2.3 m above the tank bottom is

shown in Table 3.9. The calculated slurry density at this location is 1.006 g/mL, still much larger than the 0.996 g/mL 4.3 m above the bottom (at the surface of the original supernatant liquid) after one simulation hour.

Similar to Case 3, the C-106 plume slides horizontally to deposit many of its solids when it has descended to the AY-102 sludge surface. This is shown in Figures 3.24 and 3.25 for Solids #1 and 9, just above the AY-102 sludge surface. These figures are very similar to those of Case 3, showing the finer solids accumulating around the areas the four slurry jets hit and along the wall. The solids deposited much smaller amounts around the tank center. The coarser solids tend to show the opposite trend.

Table 3.9. Predicted Reduction of C-106 Solids at the Farthest Wall in Case 4 after 1 hr of Slurry Transfer

Solid	Solids Loading at Injection (kg/m^3)	Solids Loading at Tank Wall (kg/m^3)	Reduction Factor
Solid #1	39.4	2.72	14.5
Solid #2	22.9	1.61	14.3
Solid #3	54.1	3.67	14.7
Solid #4	61.5	4.15	14.8
Solid #5	54.7	3.65	15.0
Solid #6	61.9	3.92	15.8
Solid #7	22.5	1.22	18.4
Solid #8	24.0	0.79	30.3
Solid #9	16.7	0.22	77.2
Total	368.6	21.95	16.8

The estimated variation of the solid accumulation for Case 4 is shown in Table 3.10. The depth variation is similar to Case 3 and smaller than Case 2. The estimated maximum accumulated depth is 10% more than the average accumulated depth, which, in turn, is 2.4% less than the depth accumulated at riser 15S, again indicating the accuracy of the Enraf densitometer reading. The maximum depth would be 7% greater than the depth at riser 15S in this case.

Table 3.10. Estimated Depth Variation of C-106 Solid Accumulation in Tank AY-102, Case 4, after 1 hr of Slurry Transfer

Maximum Solid Volume Fraction	Solid Volume Fraction at Riser 15S	Average Solid Volume Fraction	Ratio of Maximum Depth to Average Depth	Ratio of Average Depth to Depth at Riser 15S	Ratio of Maximum Depth to Depth at Riser 15S
0.0419	0.0390	0.0381	1.10	0.976	1.07

3.5 Case 5: 30 wt% Slurry in 5.0-m AY-102 Waste

The 300-gpm discharge of the 30-wt% slurry into AY-102 was simulated previously with TEMPEST (Whyatt et al. 1996). This case used data from a C-106 Tank Characterization Report (Castaing 1994) that shows the C-106 particle sizes as being 5 to 55 μm, as shown in Table 2.2. The C-106 slurry, with 1.210 g/mL density, is injected into the AY-102 supernatant liquid with 0.990 g/mL density in this case. Solid concentrations in the C-106 slurry with 30 wt% solid at injection nozzles for this case are shown in Table 3.11. The test results for Case 5, as explained by the following text, estimated the maximum accumulated depth is 2% greater than the depth measured at riser 15S.

Table 3.11. Solid Concentrations at Injection Nozzles in Case 5 after 1 hr of Slurry Transfer

Solid	#1	#2	#3	#4	#5	#6	#7	#8	#9
Concen-tration kg/m^3	130	39.9	18.1	43.5	17.5	29.0	39.2	26.8	22.2

Similar to Cases 3 and 4, the slurried solids, immediately after they are expelled from the 1-in. nozzles, sink very rapidly toward the bottom because of the much greater density of the 30 wt% slurry. As expected from the ratio of solid fall velocity to jet velocity and solid concentrations, all solids behave as a part of the negative plume, rather than individual solids settling toward the tank bottom.

Figures 3.26 and 3.27 show the predicted vertical distributions of concentrations of Solids #1 (5–10-μm diameter) and 9 (50–55-μm diameter) after one simulation hour (Whyatt et al. 1996). These figures show Solids #1 and 9 descending very rapidly, with the plume centers hitting the bottom. The slurry plume in this case is diluted such that by the time it is 3.4 m from the injection nozzle and 3.4 m above tank bottom, the density of the plume (1.004 g/mL) becomes the same as that just below the jet; it has lost its negative buoyancy. The jet plume descends toward the bottom until it is 4.9 m from the injection nozzle and 1.22 m above the bottom. There, the diluted jet center velocity is 0.22 m/s. The jet then starts to spread horizontally, hitting the farthest tank wall 0.84 m above the tank bottom. Near this wall, the density is 1.010 kg/mL and the jet velocity is approximately 0.04 m/s—240 times less than the initial injection velocity of 9.34 m/s.

The vertical variation of solid concentration for this case show is still large, as in Cases 3 and 4. For example, Solid #1 displays its concentrations above the settled solid layer with about 200-fold vertical variation. Within the depth below the injection nozzle (3.95 m above tank bottom), Solids #1 and 9 display vertical variations of five-fold and 18 orders of magnitude, respectively. The horizontal variations at a given depth are much smaller.

Near the farthest tank wall, where the plume hits, the initial slurry is diluted 13.3 times, which is less than in Cases 3 and 4. Dilution of each solid at the farthest tank wall, 0.84 m above the tank bottom, is shown in Table 3.12. The calculated slurry density at this location increased to 1.010 g/mL, much larger than the 0.9934 g/mL 6.4 m above bottom (the surface of the original

supernatant liquid) after one simulation hour. As in Cases 3 and 4, this density difference makes it difficult for the slurry to move upward and prevents much of the solids from being recirculated to Tank C-106 quickly, as indicated in Figures 3.26 and 3.27 where a very small amount of solids is found at the supernatant liquid surface.

Similar to Cases 3 and 4, the C-106 plume slides horizontally when it approaches the AY-102 sludge surface and deposits many of the solids it is carrying. This is shown in Figures 3.28 and 3.29 for Solids #1 and 9 just above the AY-102 sludge surface. These figures show the finer solids accumulating around the areas the four slurry jets hit. The coarser solids accumulate more in the area into which the reflected slurry is moving, including that between the area of the original slurry jet passage and the tank center.

Table 3.12. Predicted Reduction of C-106 Solids at the Farthest Tank Wall, Case 5, after 1 hr of Slurry Transfer

Solid	Solids Loading at Injection (kg/m^3)	Solids Loading at Tank wall (kg/m^3)	Reduction Factor
Solid #1	130.0	11.00	11.8
Solid #2	39.9	3.43	11.6
Solid #3	18.1	1.54	11.7
Solid #4	43.5	3.49	12.5
Solid #5	17.5	1.36	12.9
Solid #6	29.0	1.62	17.9
Solid #7	39.2	2.38	16.5
Solid #8	26.8	1.52	17.7
Solid #9	22.2	1.12	19.8
Total	366.2	27.451	13.3

The estimated variation of the solid accumulation for Case 5 is shown in Table 3.13. The depth variation is similar to but slightly smaller than that of Case 4. The estimated maximum accumulated depth for Case 5 is 7% more than the average accumulated depth, which, in turn, is 4.5% less than the depth accumulated at riser 15S, demonstrating the accuracy of the Enraf. The maximum depth would be 2% greater than the depth at riser 15S in this case.

Table 3.13. Estimated Depth Variation of C-106 Solid Accumulation in Tank AY-102, Case 5, after 1 hr of Slurry Transfer

Maximum Solid Volume Fraction	Solid Volume Fraction at Riser 15S	Average Solid Volume Fraction	Ratio of Maximum Depth to Average Depth	Ratio of Average Depth to Depth at Riser 15S	Ratio of Maximum Depth to Depth at Riser 15S
0.0473	0.0465	0.0444	1.07	0.955	1.02

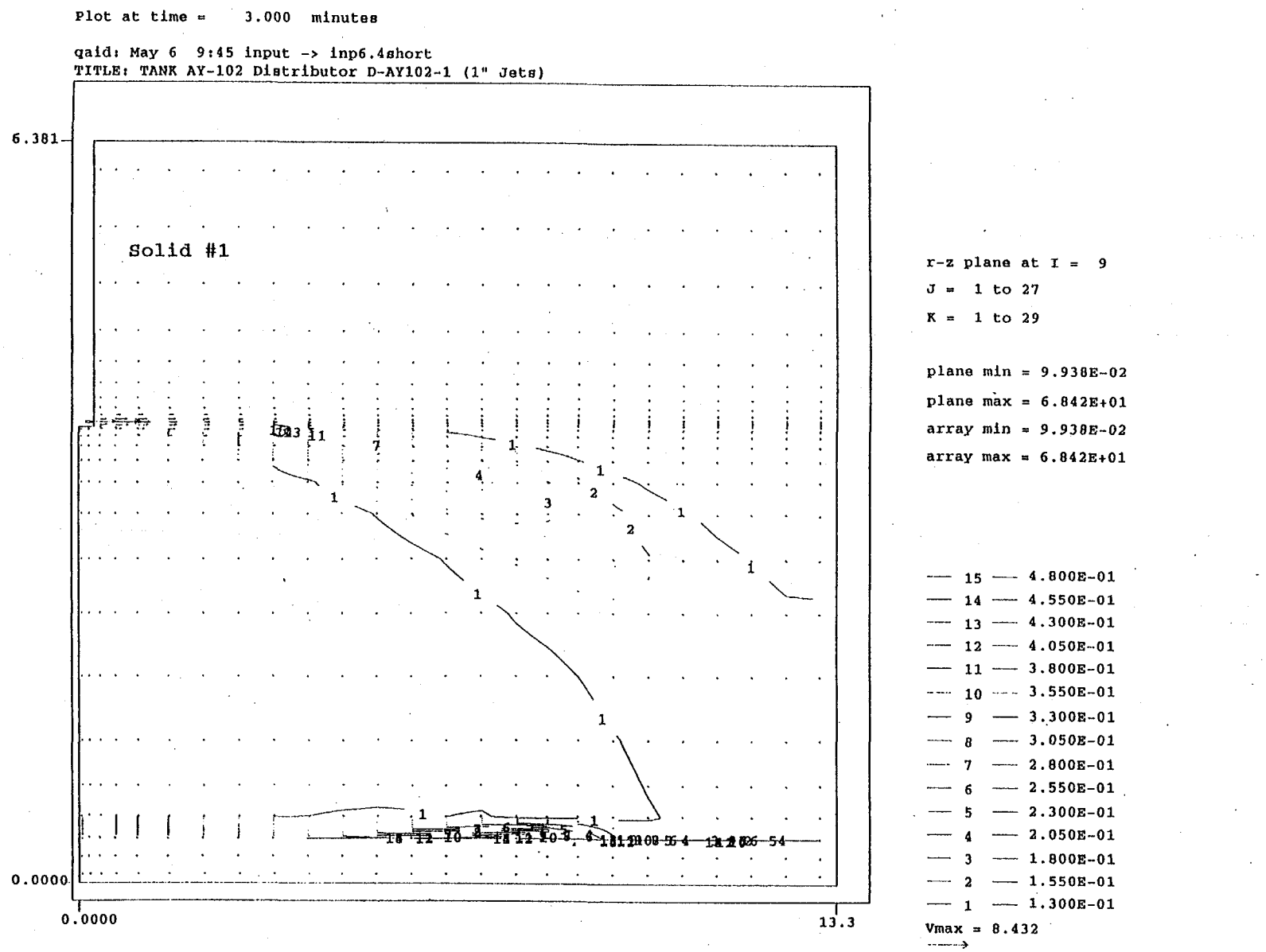

Figure 3.1. Predicted Vertical Distribution of Flow and Solid #1 Concentration on a Vertical Plane Containing One of the Nozzles in Tank AY-102 at Three Simulation Minutes, Case 1

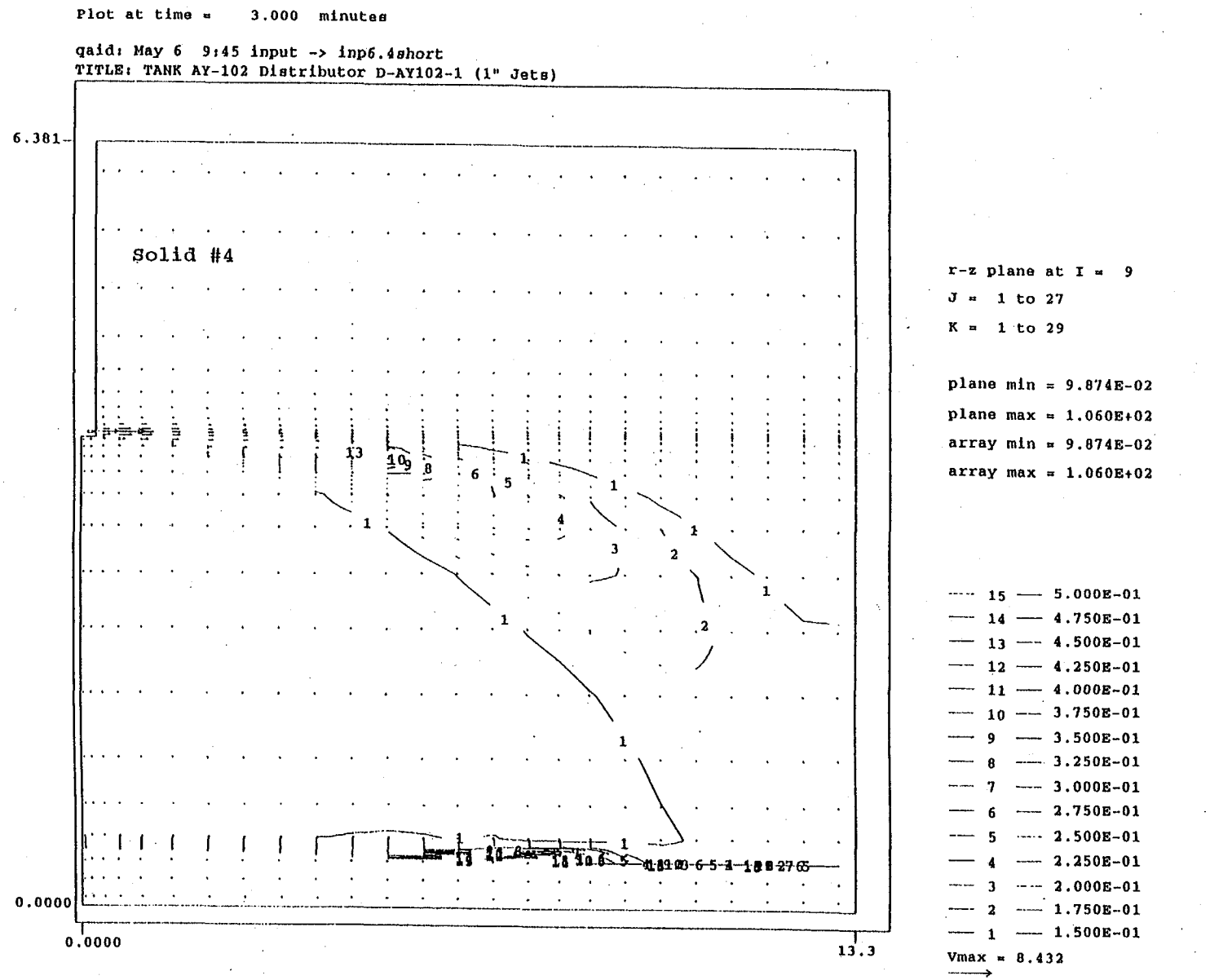

Figure 3.2. Predicted Vertical Distribution of Flow and Solid #4 Concentration on a Vertical Plane Containing One of the Nozzles in Tank AY-102 at Three Simulation Minutes, Case 1

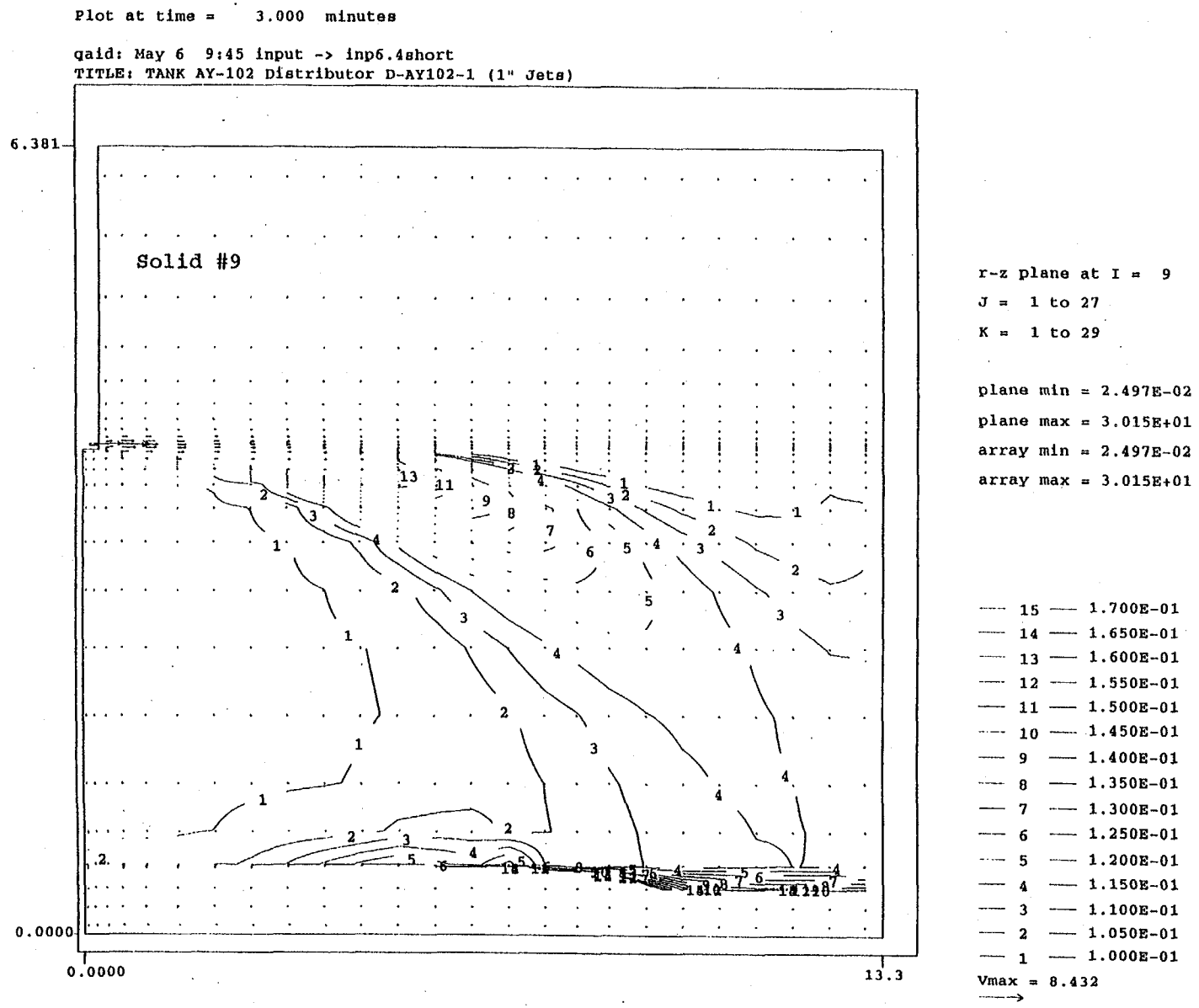

Figure 3.3. Predicted Vertical Distribution of Flow and Solid #9 Concentration on a Vertical Plane Containing One of the Nozzles in Tank AY-102 at Three Simulation Minutes, Case 1

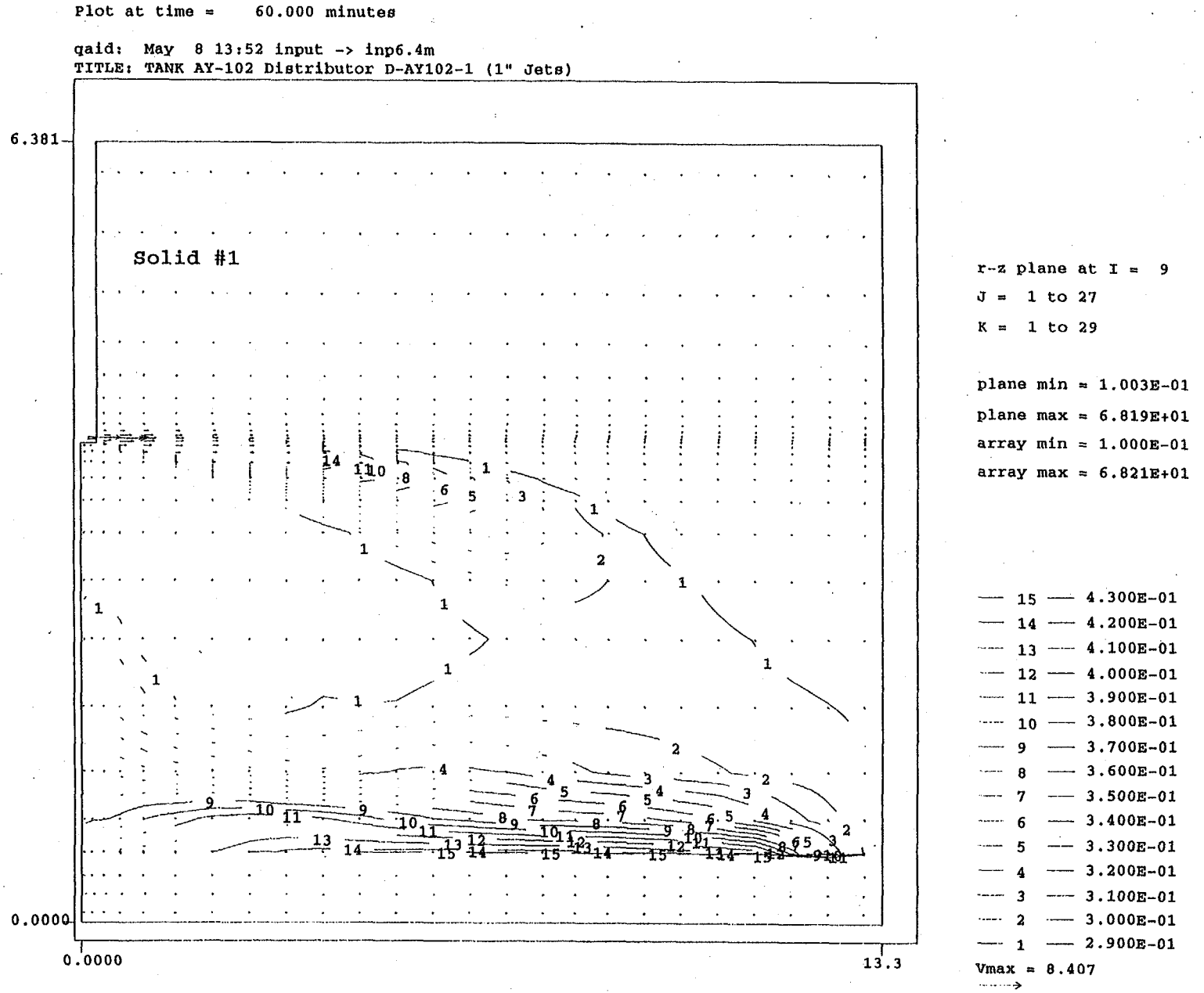

Figure 3.4 Predicted Vertical Distribution of Flow and Solid #1 Concentration on a Vertical Plane Containing One of the 1-in. Nozzles in Tank AY-102 One Simulation Hour, Case 1

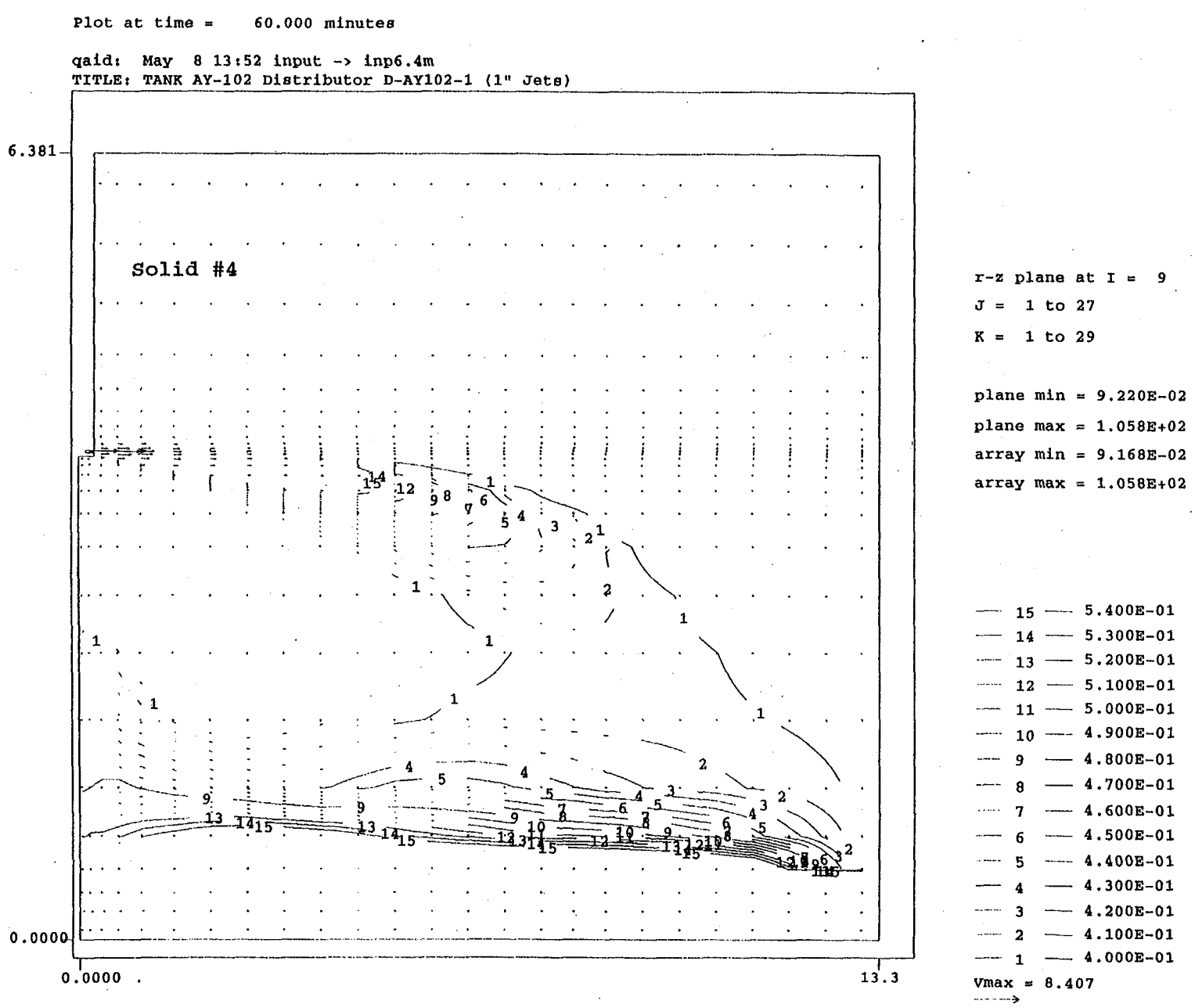

Figure 3.5. Predicted Vertical Distribution of Flow and Solid #4 Concentration on a Vertical Plane Containing One of the 1-in. Nozzles in Tank AY-102 at One Simulation Hour, Case 1

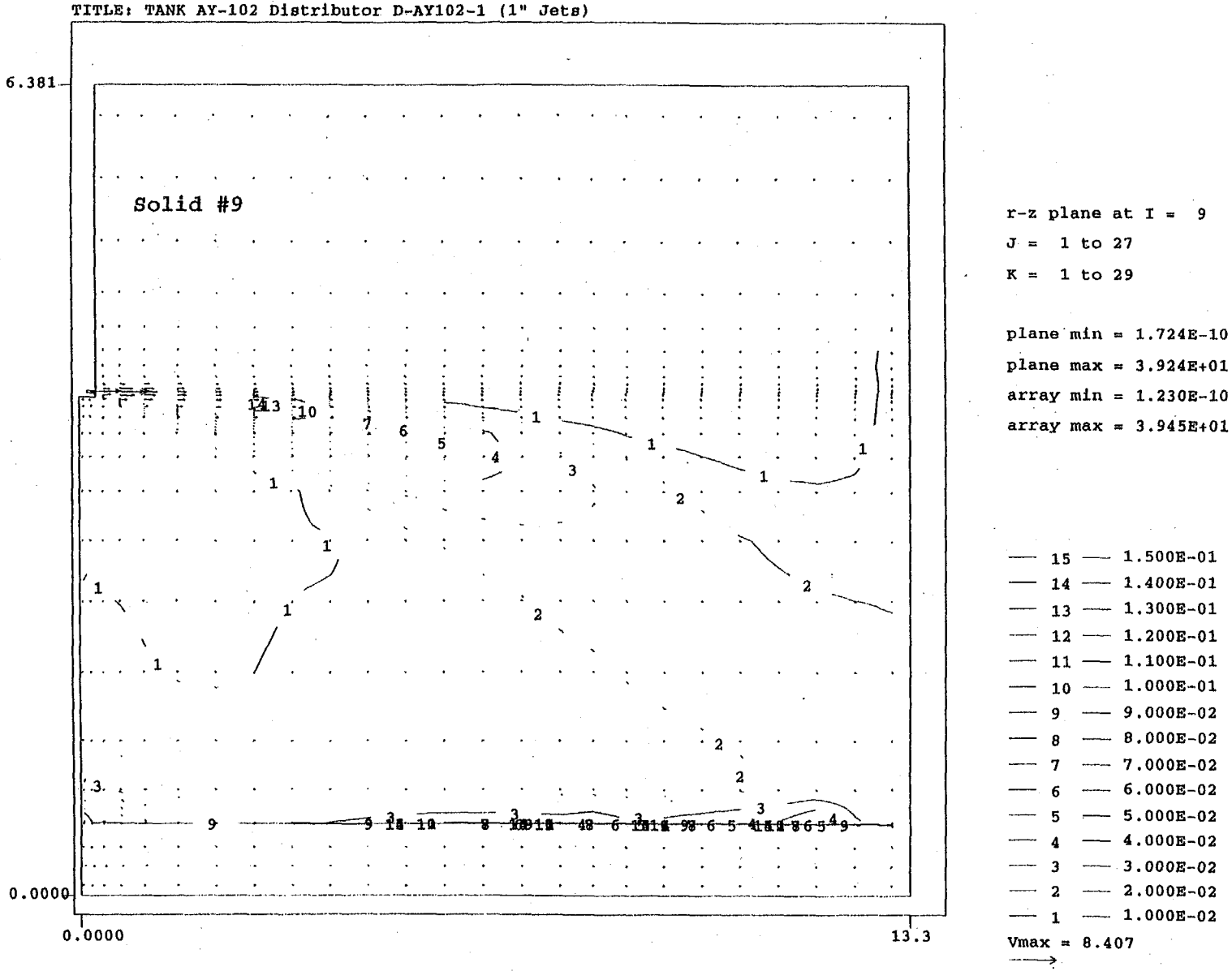

Figure 3.6. Predicted Vertical Distribution of Flow and Solid #9 Concentration on a Vertical Plane Containing One of the Nozzles in Tank AY-102 at One Simulation Hour, Case 1

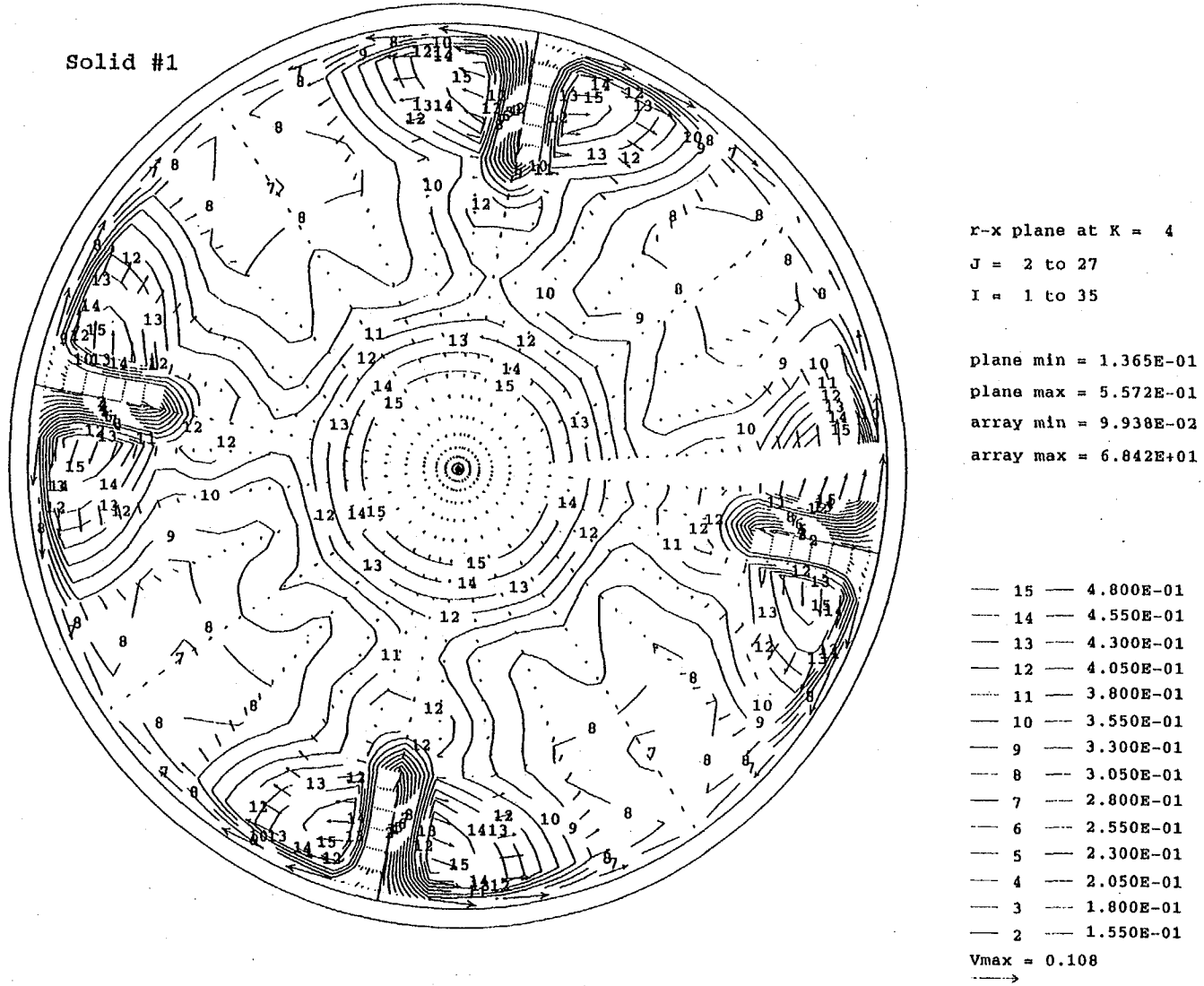

Figure 3.7. Predicted Horizontal Distributions of Flow and Solid #1 Concentration Just above the Original Sludge of Tank AY-102 at Three Simulation Minutes, Case 1

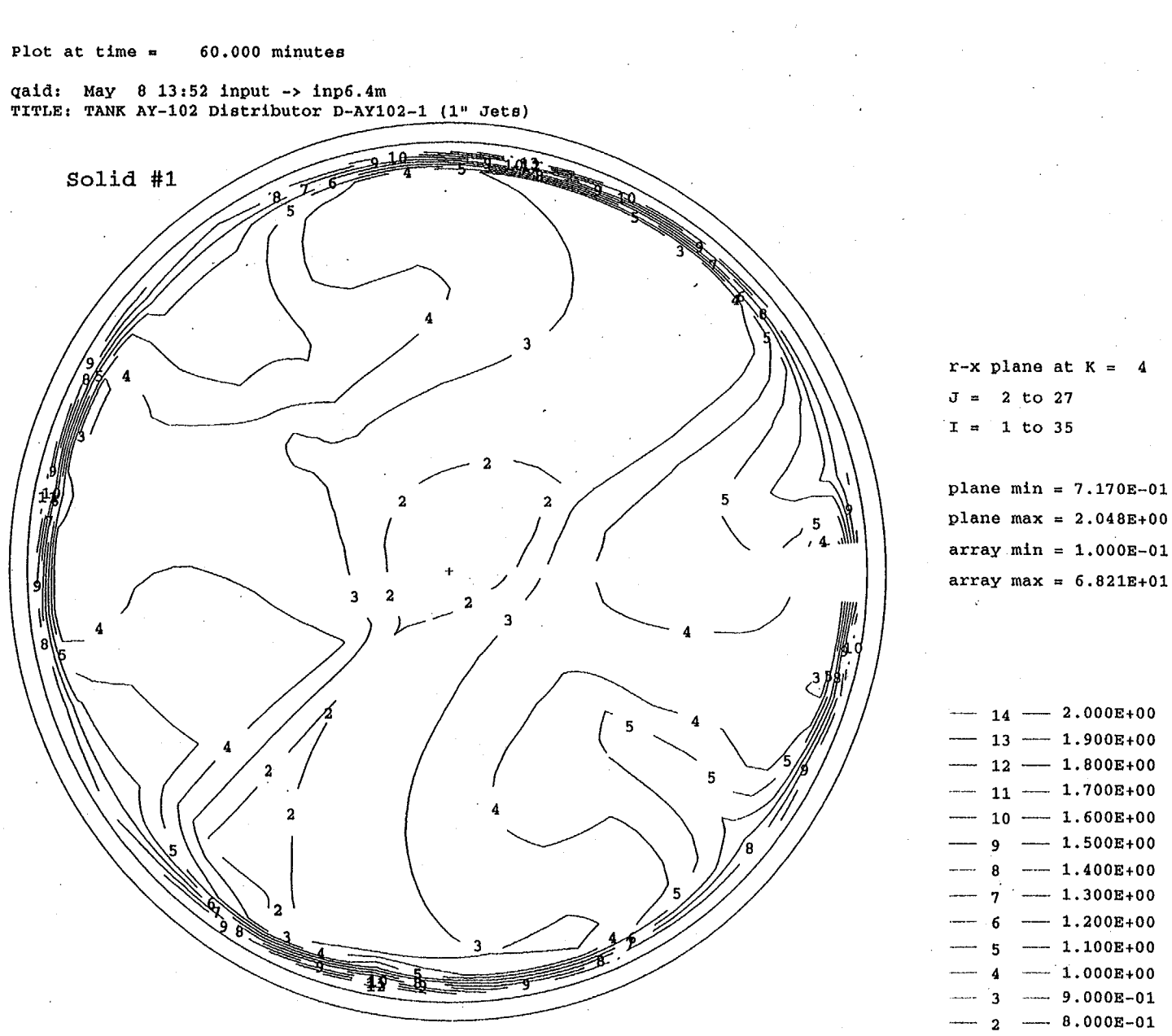

Figure 3.8. Predicted Horizontal Distributions of Flow and Solid #1 Concentration Just above the Original Sludge of Tank AY-102 at One Simulation Hour, Case 1

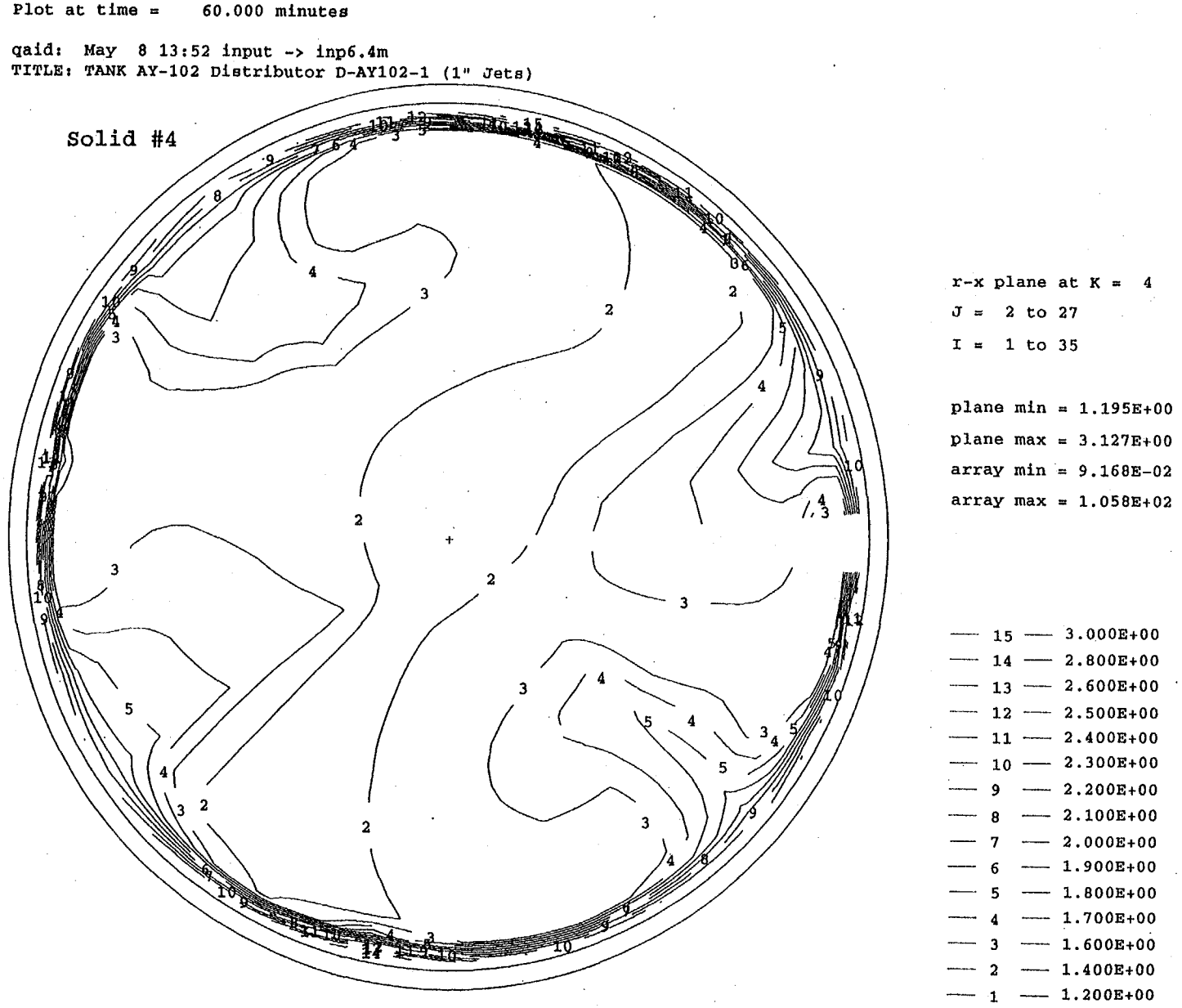

Figure 3.9. Predicted Horizontal Distributions of Flow and Solid #4 Concentration Just above the Original Sludge of Tank AY-102 at One Simulation Hour, Case 1

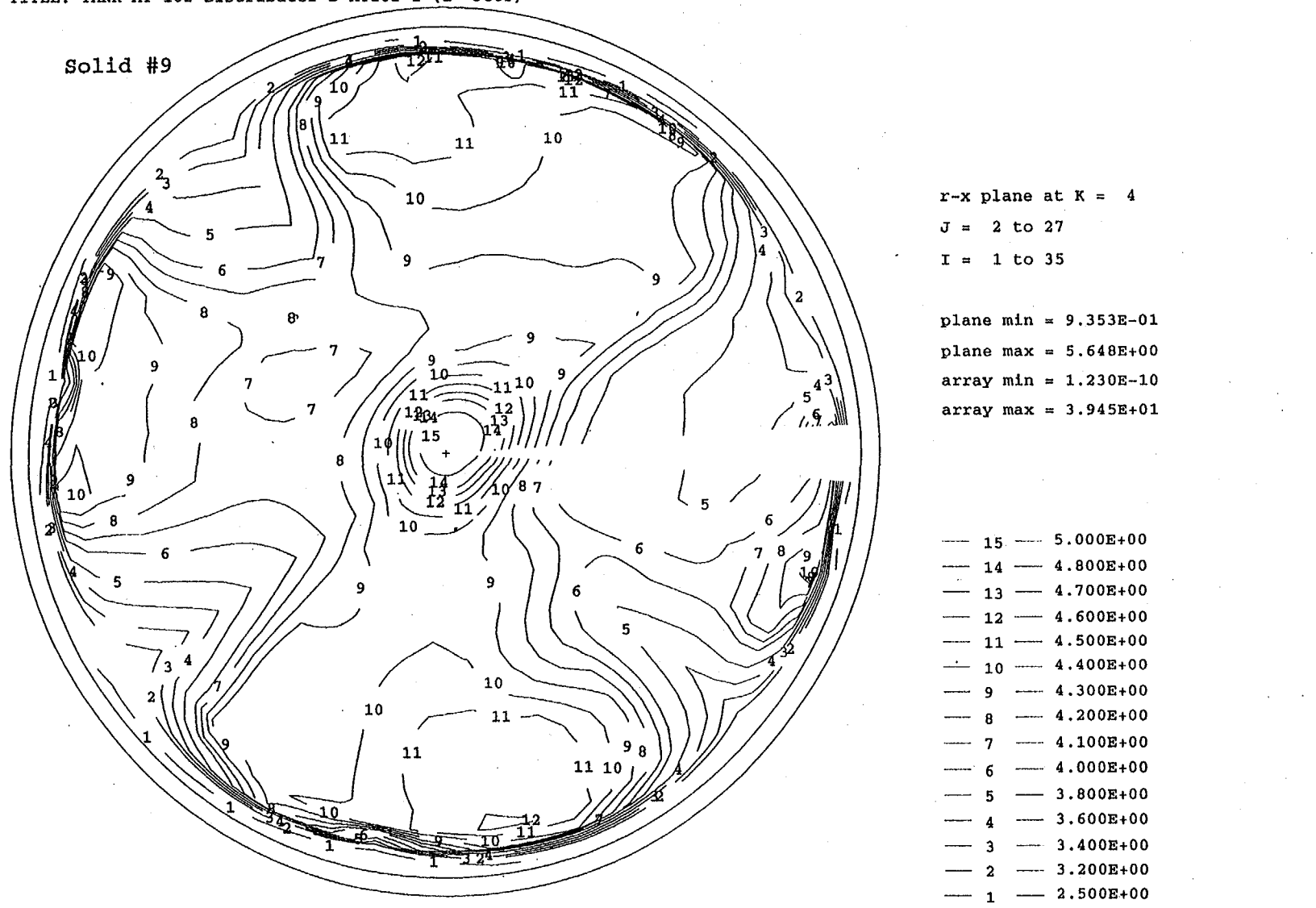

Figure 3.10. Predicted Horizontal Distributions of Flow and Solid #9 Concentration Just above the Original Sludge of Tank AY-102 at One Simulation Hour, Case 1

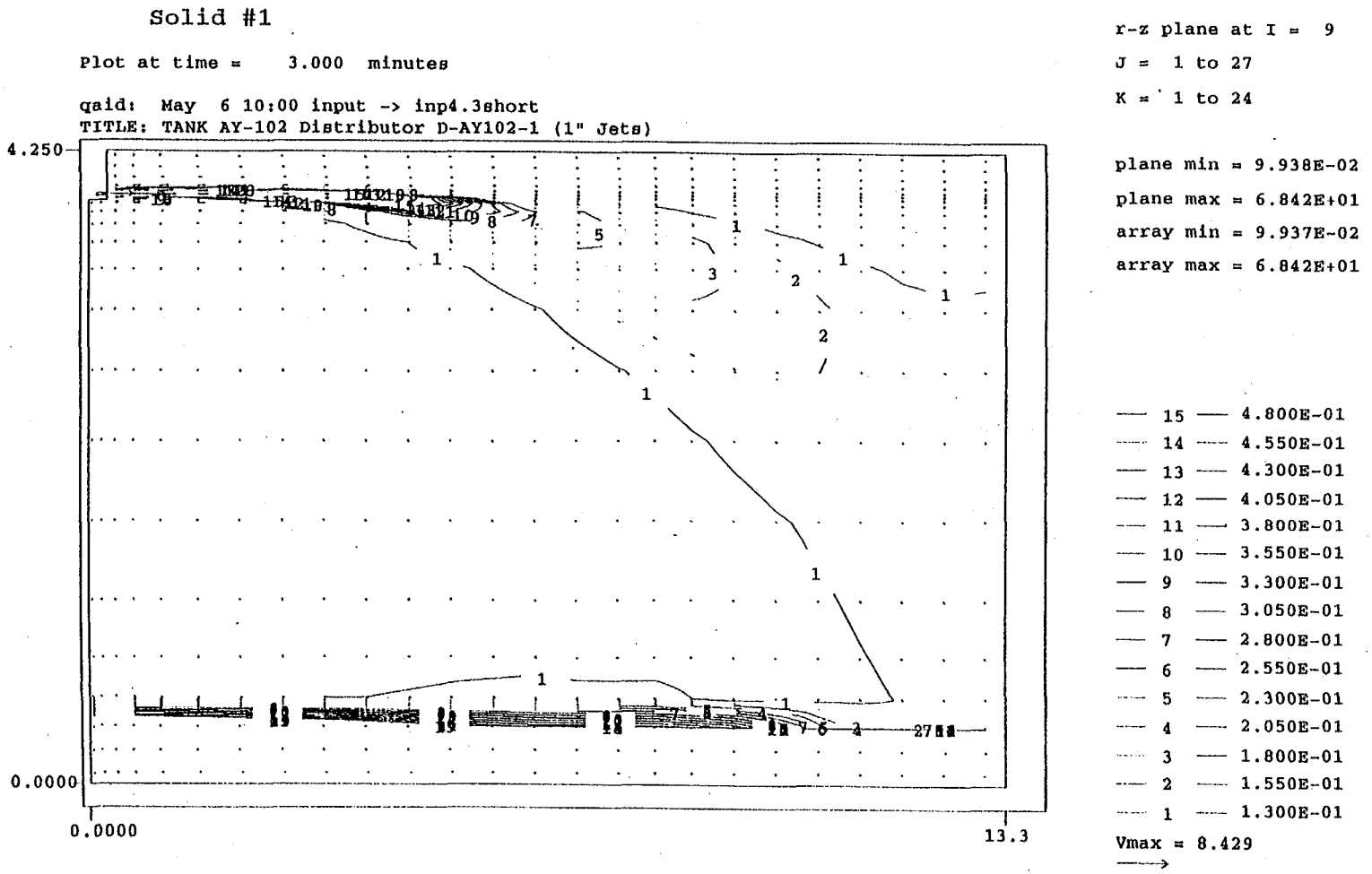

Figure 3.11. Predicted Vertical Distribution of Flow and Solid #1 Concentration on Vertical Plane Containing One of the Nozzles in Tank AY-102 at Three Simulation Minutes, Case 2

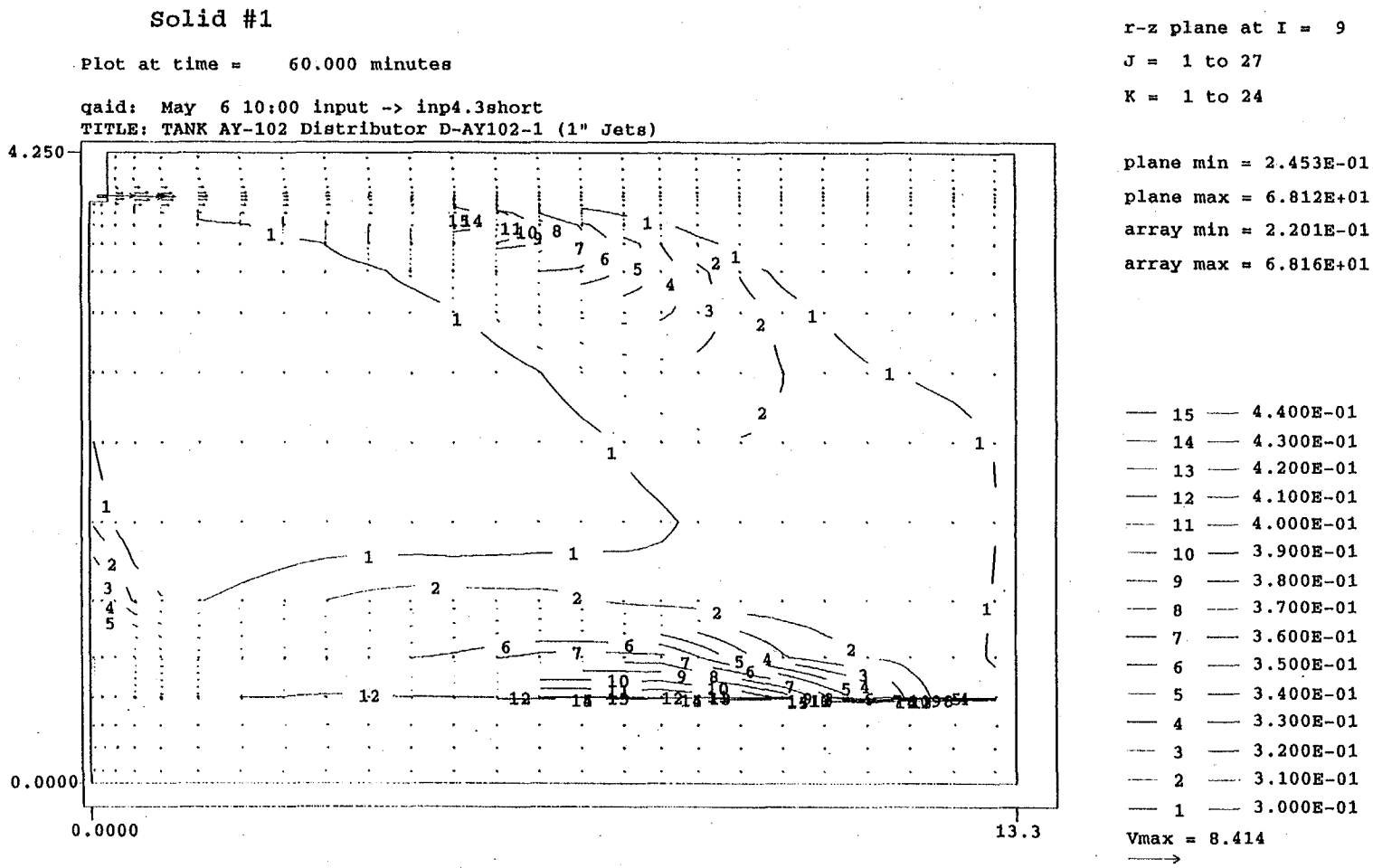

Figure 3.12. Predicted Vertical Distribution of Flow and Solid #1 Concentration on a Vertical Plane Containing One of the Nozzles in Tank AY-102 at One Simulation Hour, Case 2

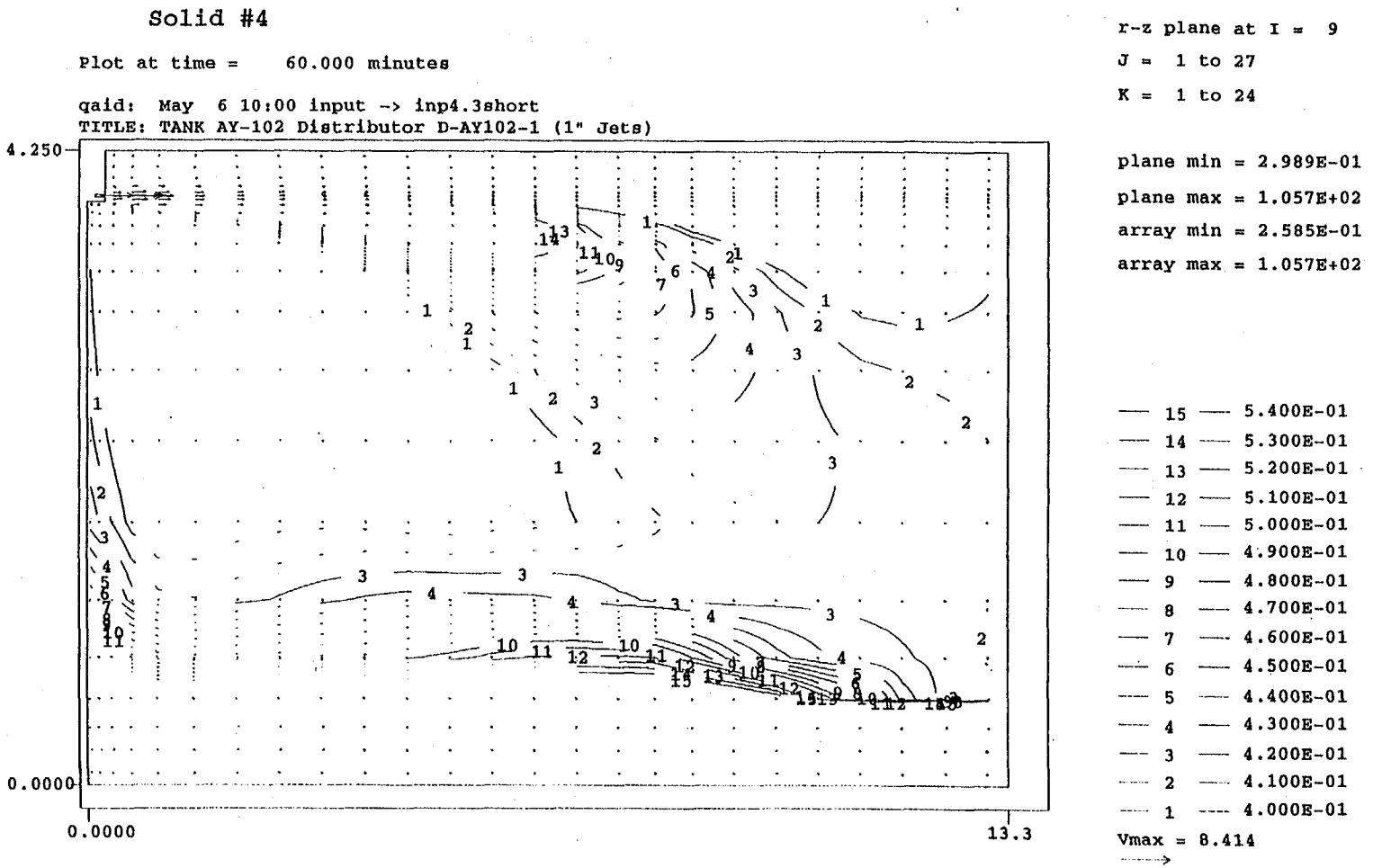

Figure 3.13. Predicted Vertical Distribution of Flow and Solid #4 Concentration on a Vertical Plane Containing One of the Nozzles in Tank AY-102 at One Simulation Hour, Case 2

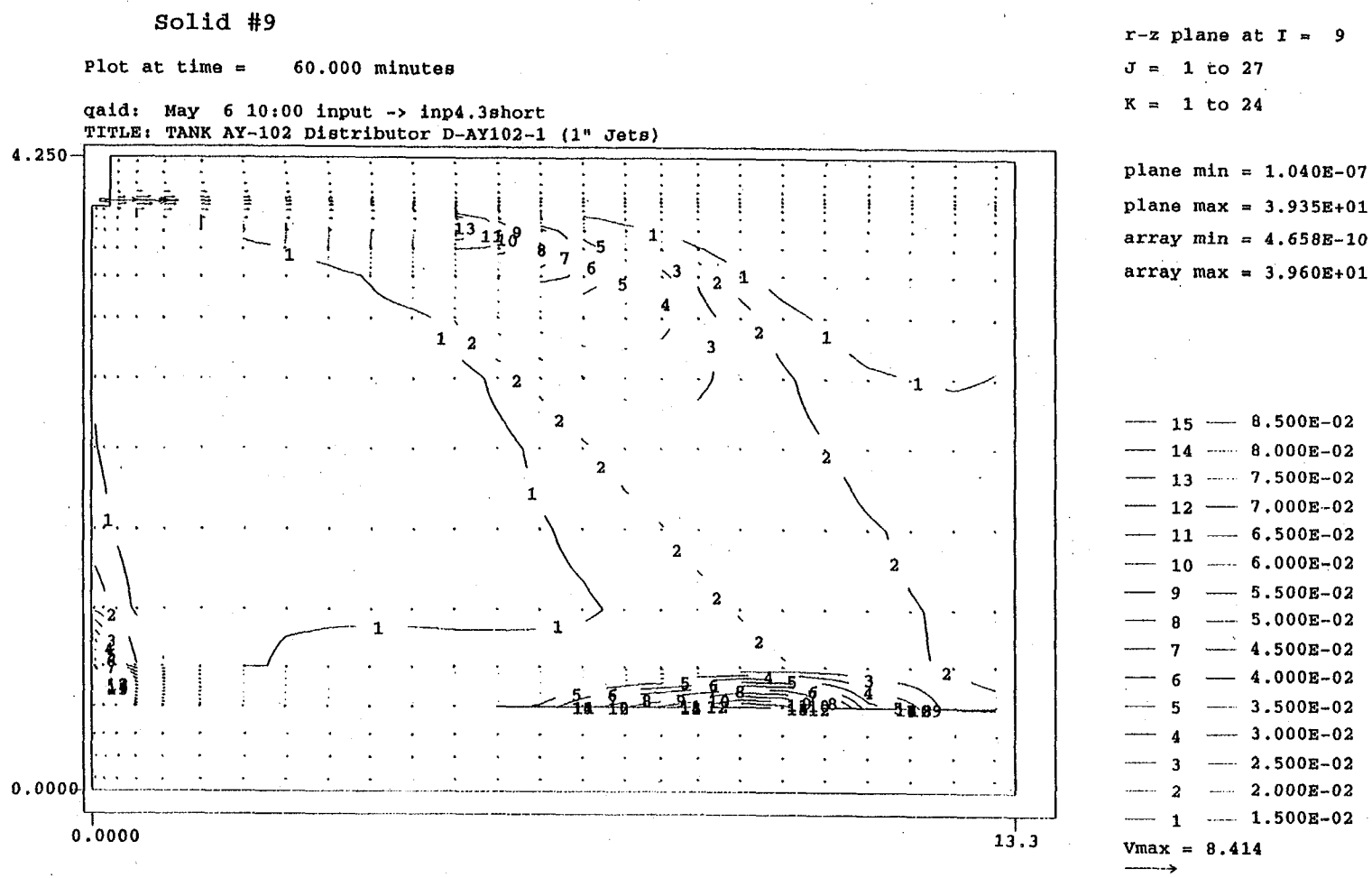

Figure 3.14. Predicted Vertical Distribution of Flow and Solid #9 Concentration on a Vertical Plane Containing One of the 1-in. Nozzles in Tank AY-102 at One Simulation Hour, Case 2

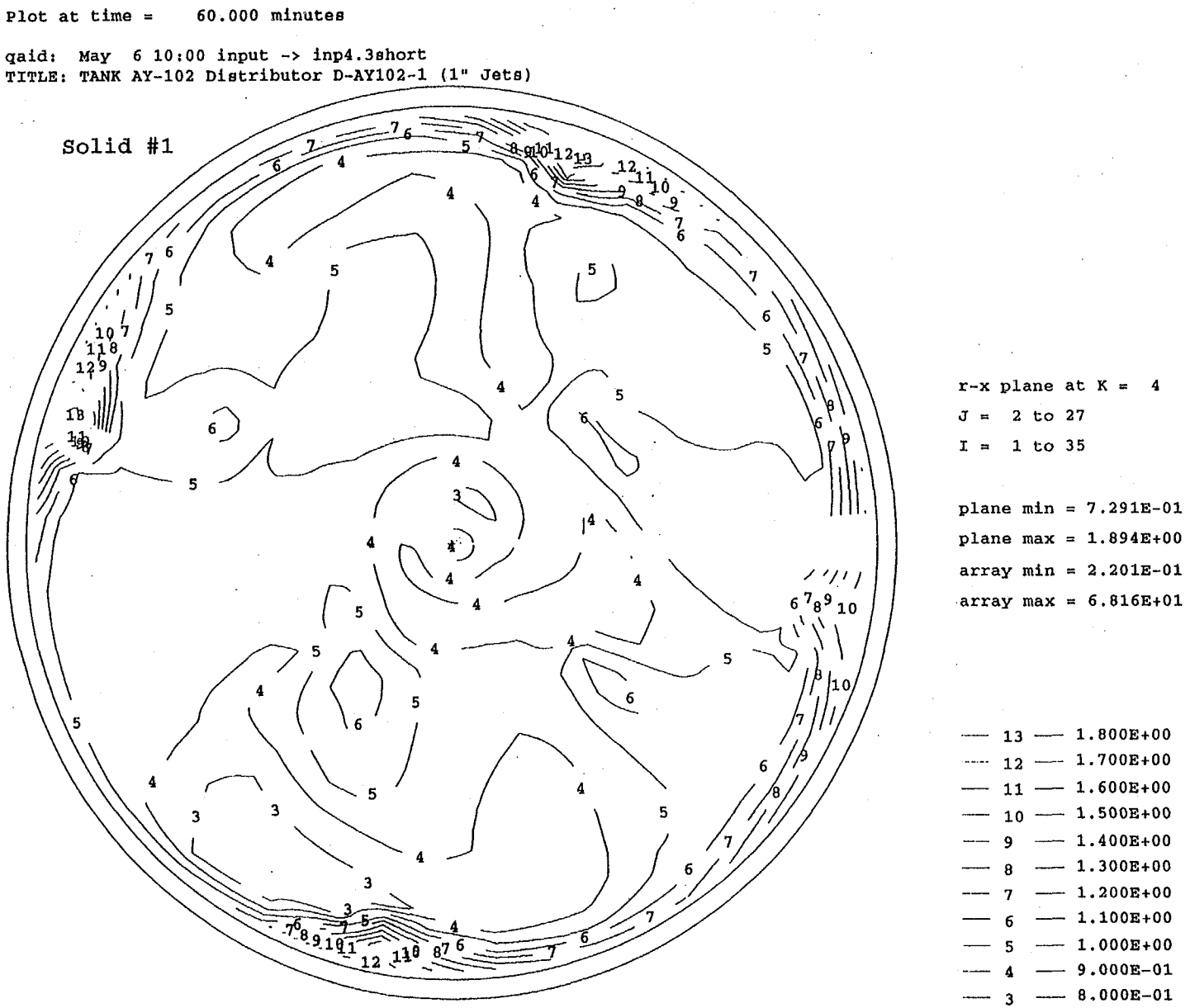

Figure 3.15. Predicted Horizontal Distributions of Flow and Solid #1 Concentration Just above the Original Sludge of Tank AY-102 at One Simulation Hour, Case 2

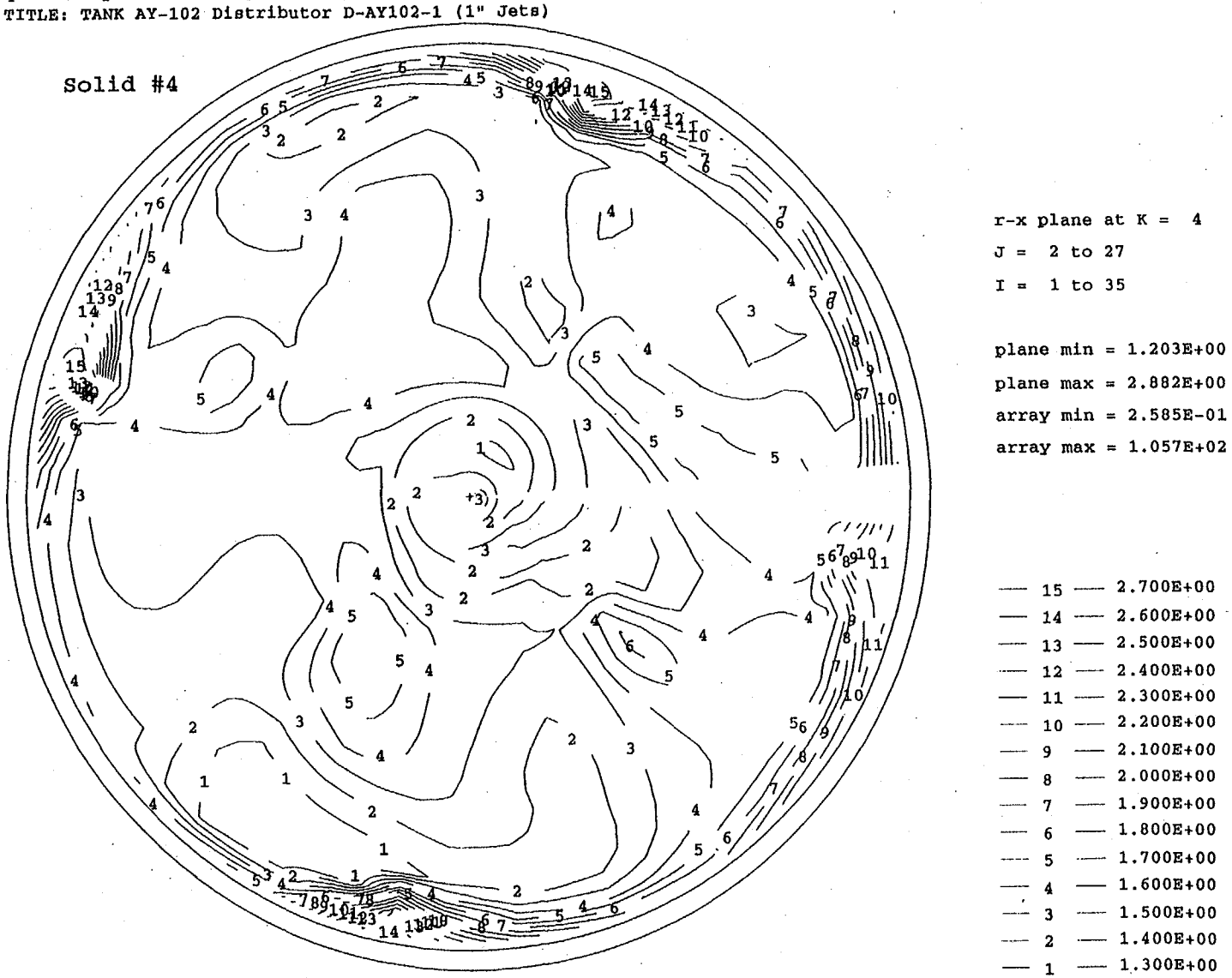

Figure 3.16. Predicted Horizontal Distributions of Flow and Solid #4 Concentration Just above the Original Sludge of Tank AY-102 at One Simulation Hour, Case 2

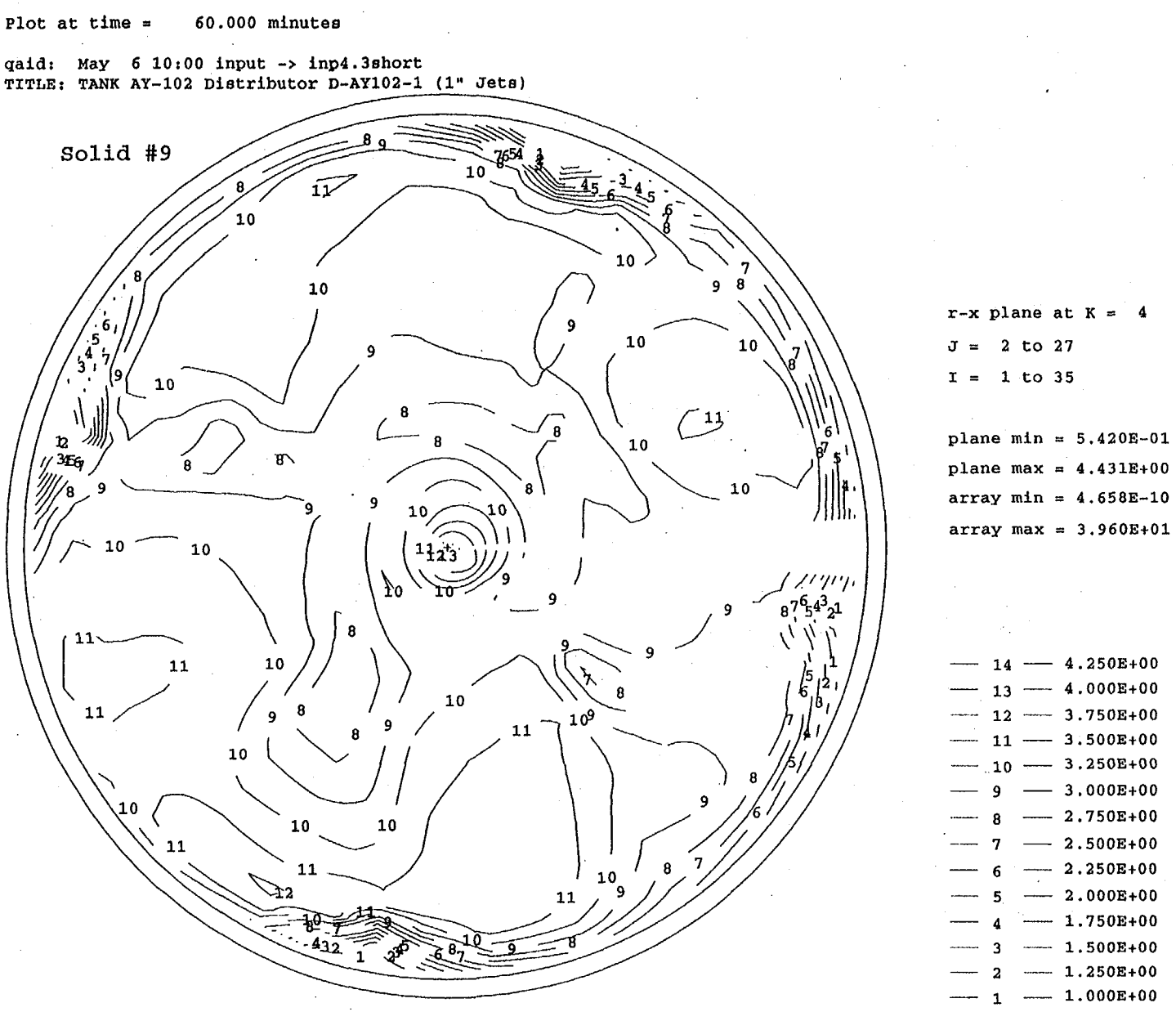

Figure 3.17. Predicted Horizontal Distributions of Flow and Solid #9 Concentration Just above the Original Sludge of Tank AY-102 at One Simulation Hour, Case 2

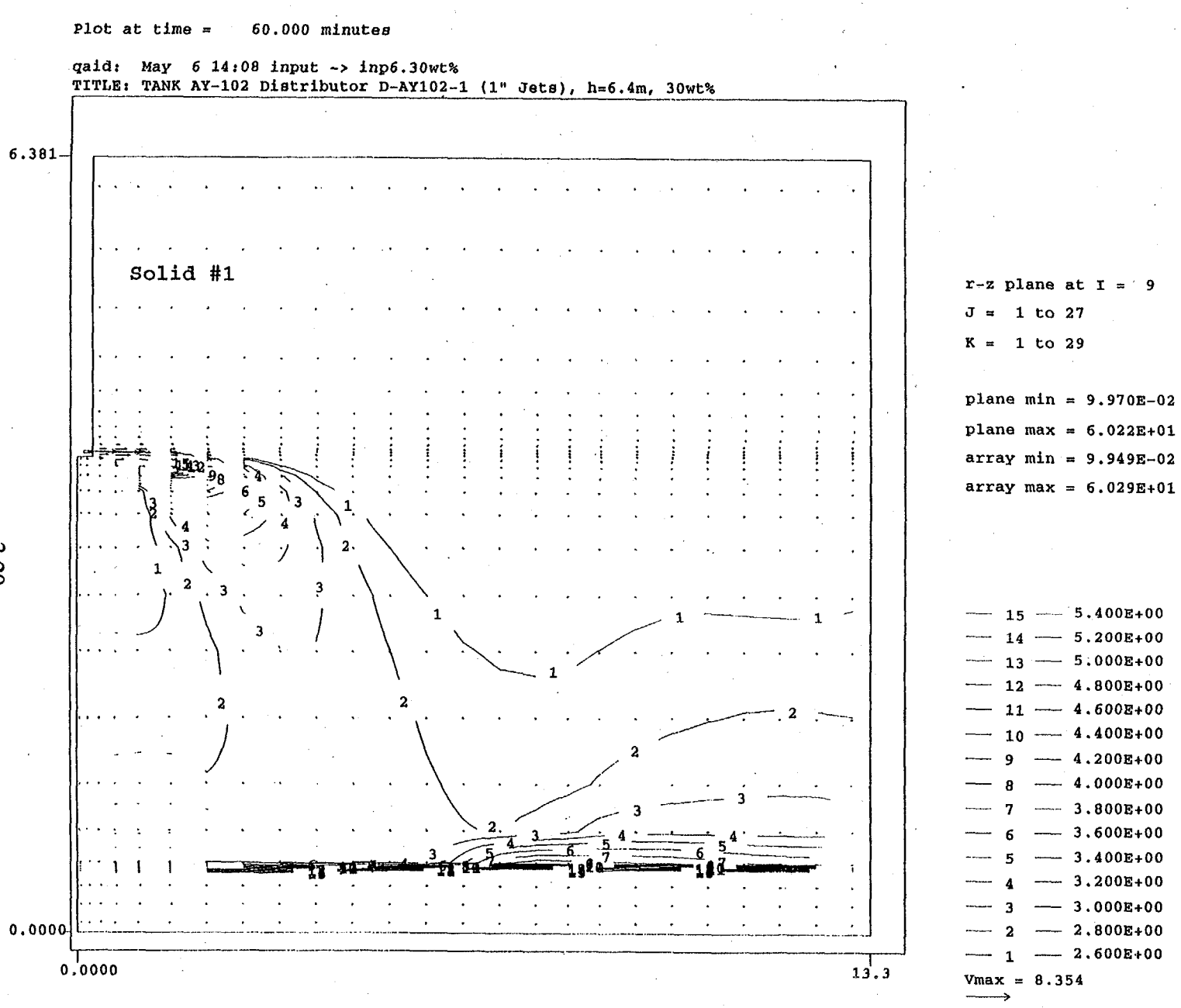

Figure 3.18. Predicted Vertical Distribution of Flow and Solid #1 Concentration on a Vertical Plane Containing One of the 1-in. Nozzles in Tank AY-102 at One Simulation Hour, Case 3

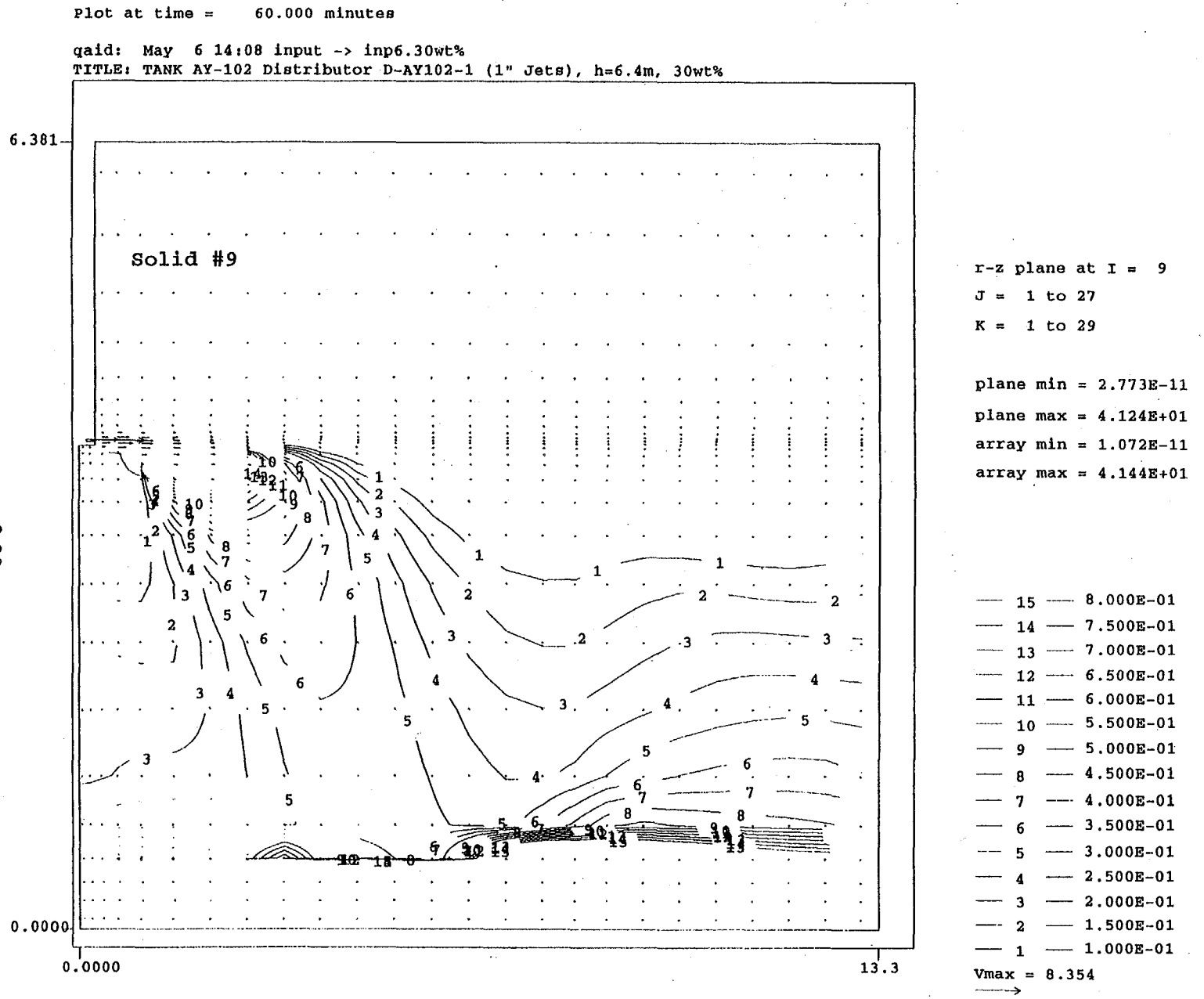

3.30

Figure 3.19. Predicted Vertical Distribution of Flow and Solid #9 Concentration on a Vertical Plane Containing One of the 1-in. Nozzles in Tank AY-102 at One Simulation Hour, Case 3

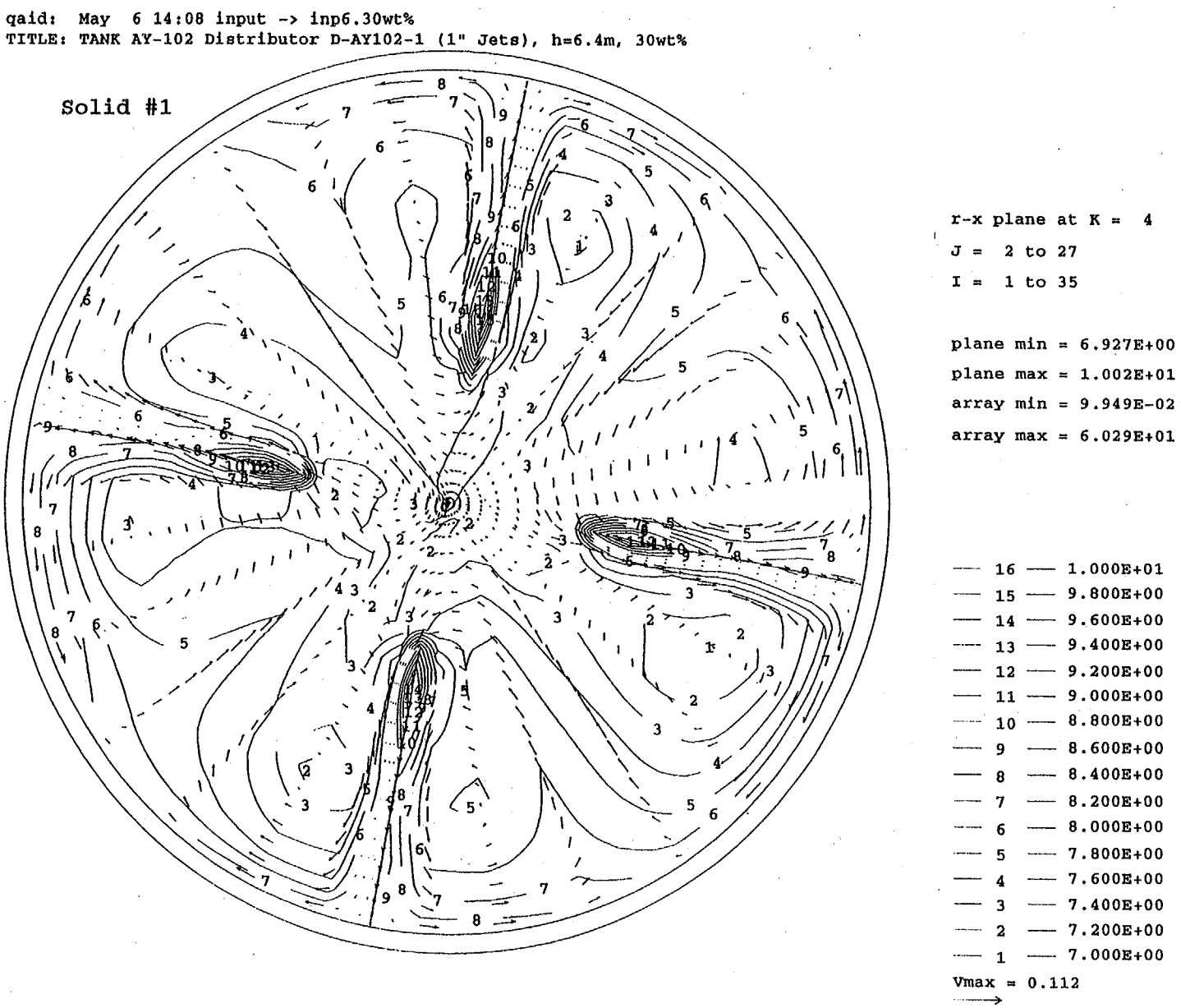

Figure 3.20. Predicted Horizontal Distributions of Flow and Solid #1 Concentration Just above the Original Sludge of Tank AY-102 at One Simulation Hour, Case 3

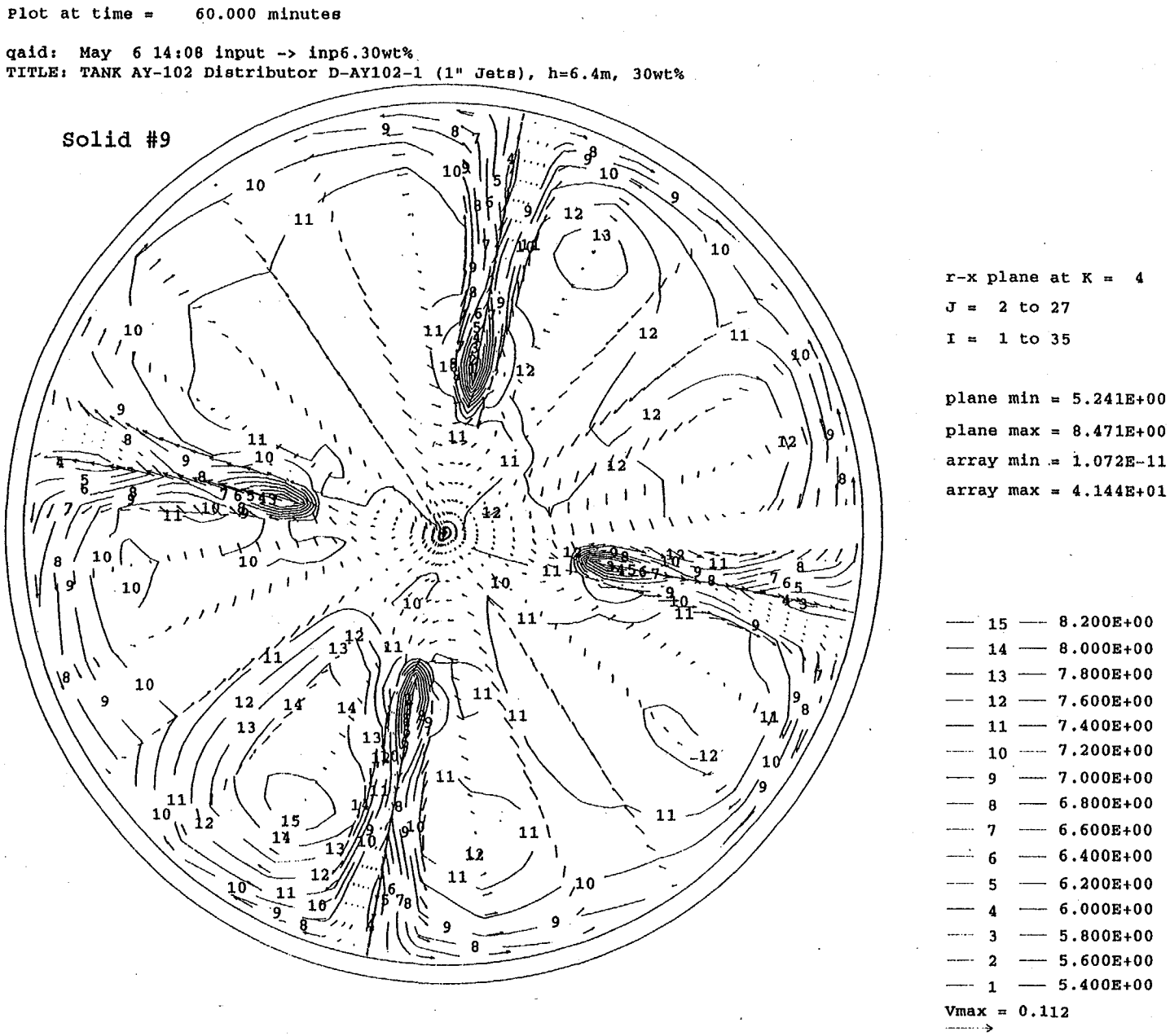

Figure 3.21. Predicted Horizontal Distributions of Flow and Solid #9 Concentration Just above the Original Sludge of Tank AY-102 at One Simulation Hour, Case 3

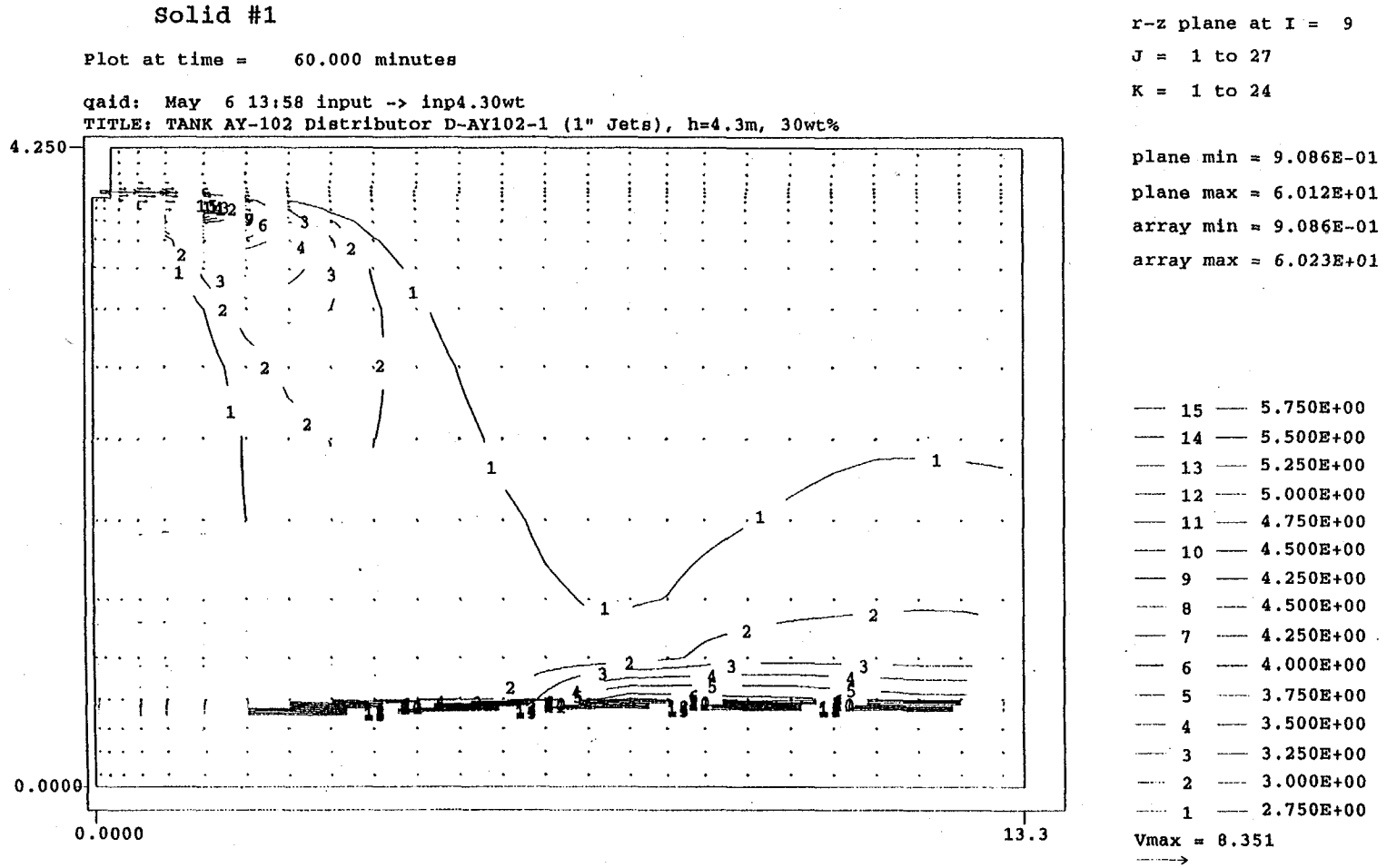

Figure 3.22. Predicted Vertical Distribution of Flow and Solid #1 Concentration on a Vertical Plane Containing One of the 1-in. Nozzles in Tank AY-102 at One Simulation Hour, Case 4

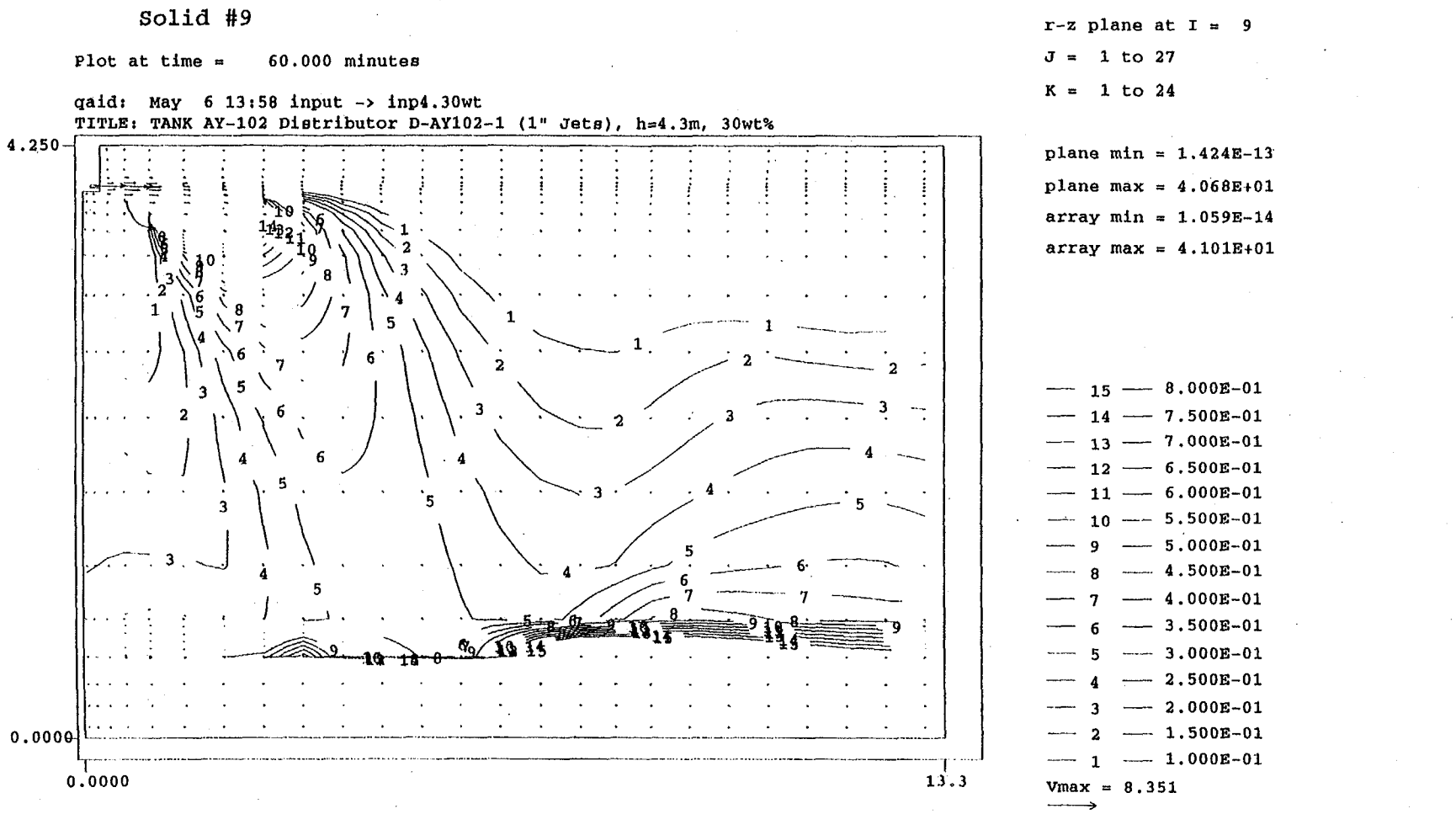

Figure 3.23. Predicted Vertical Distribution of Flow and Solid #9 Concentration on a Vertical Plane Containing One of the 1-in. Nozzles in Tank AY-102 at One Simulation Hour, Case 4

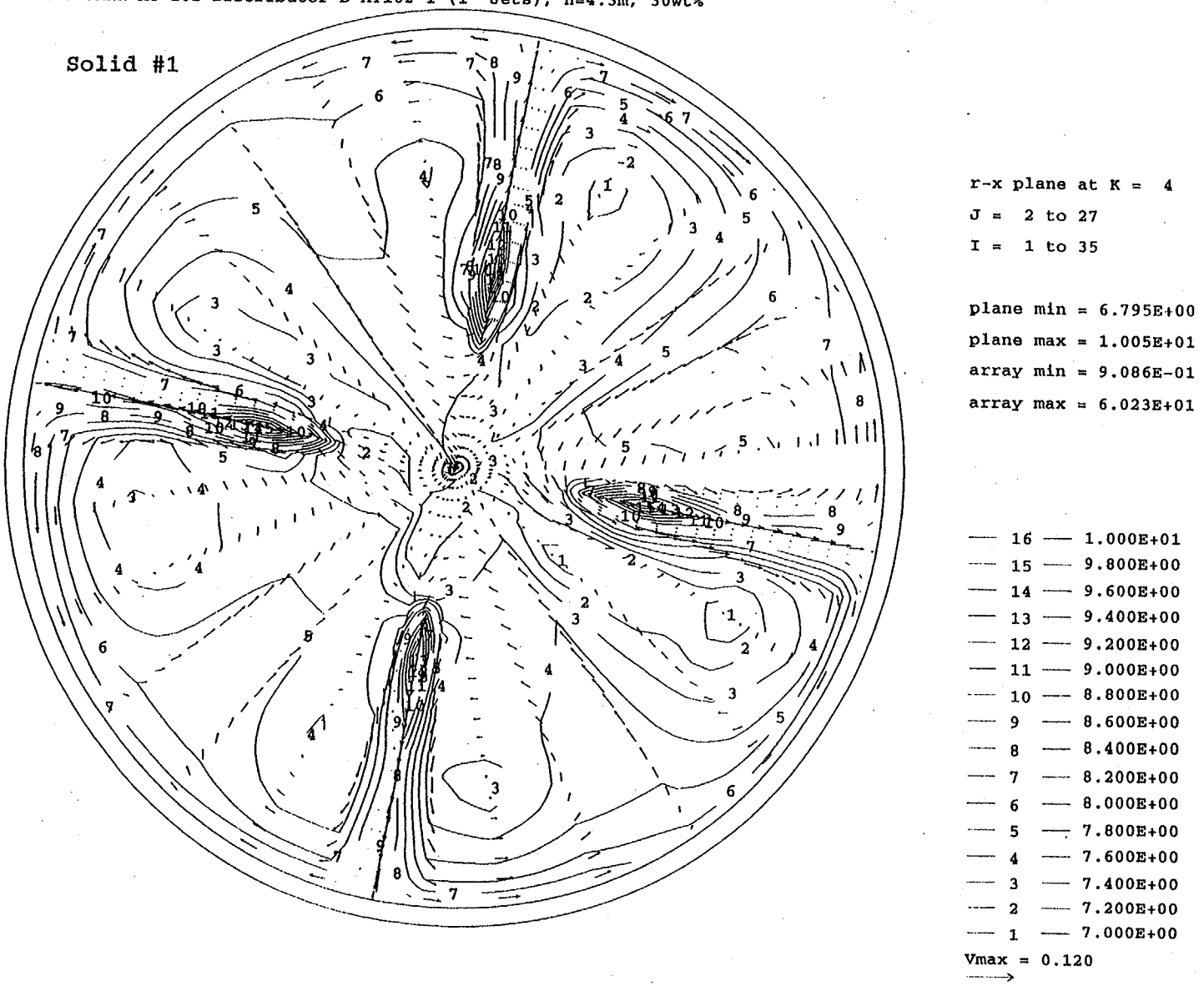

Figure 3.24. Predicted Horizontal Distributions of Flow and Solid #1 Concentration Just above the Original Sludge of Tank AY-102 at One Simulation Hour, Case 4

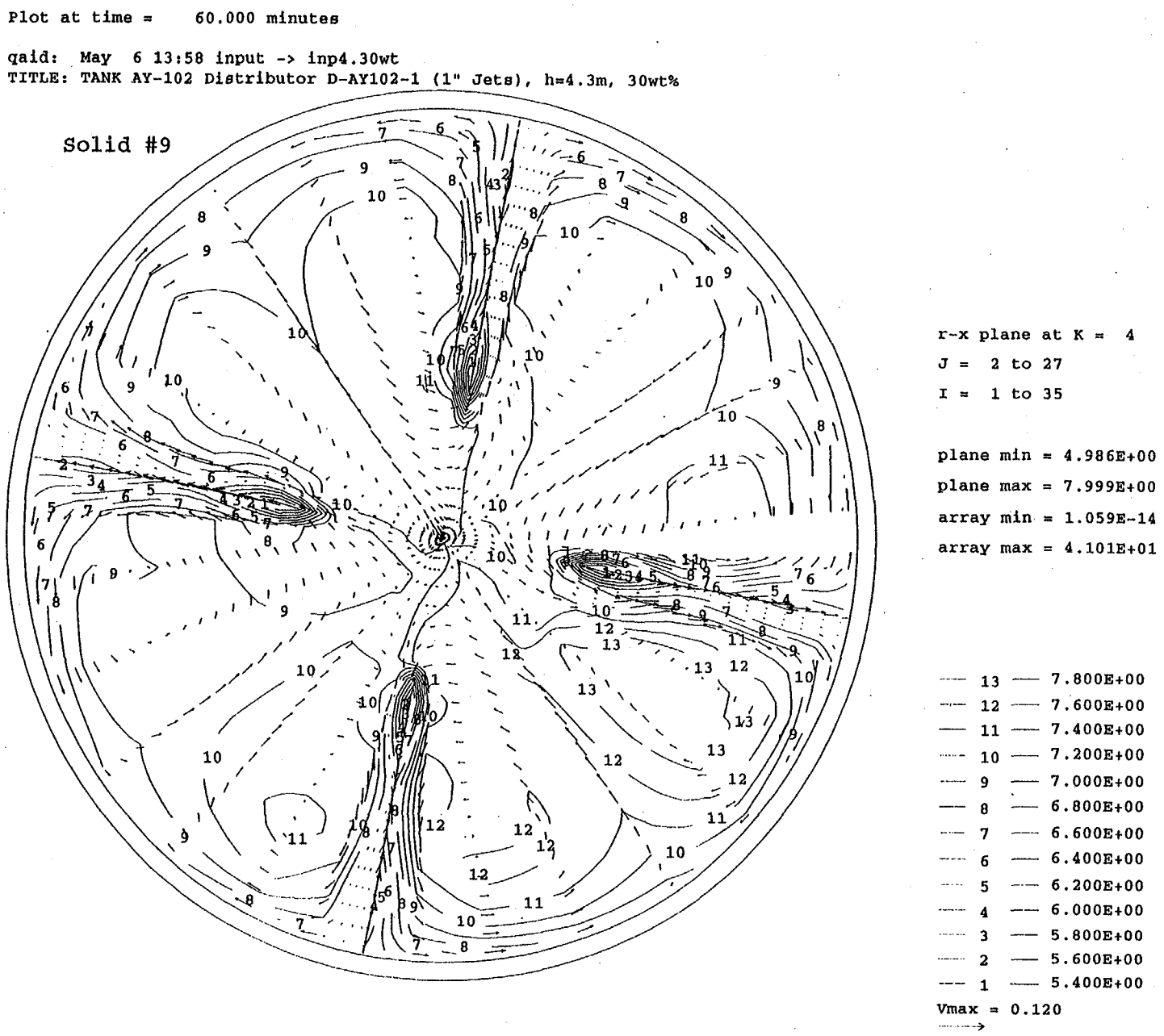

Figure 3.25. Predicted Horizontal Distributions of Flow and Solid #9 Concentration Just above the Original Sludge of Tank AY-102 at One Simulation Hour, Case 4

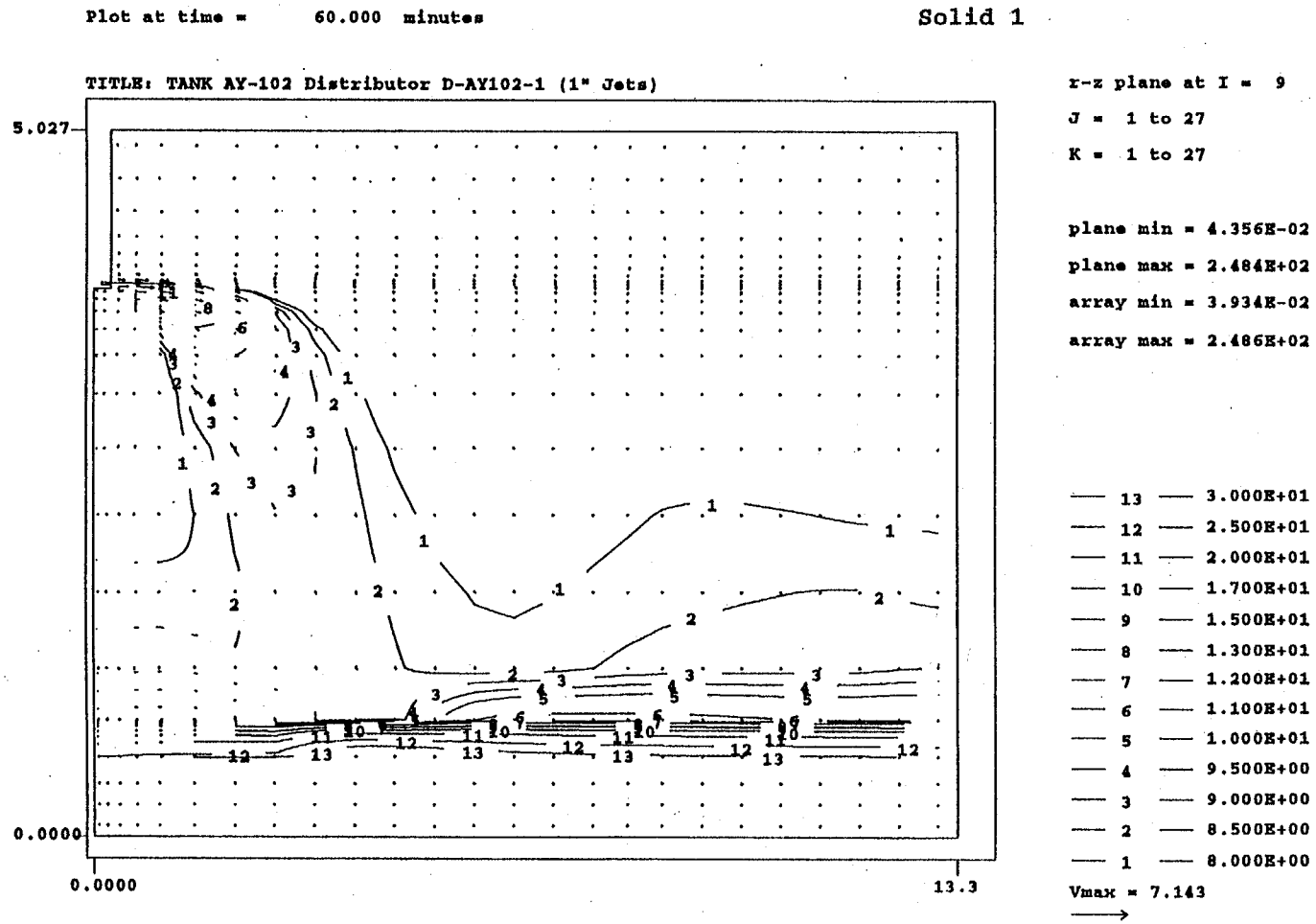

Figure 3.26. Predicted Vertical Distribution of Flow and Solid #1 Concentration on a Vertical Plane Containing One of the 1-in. Nozzles in Tank AY-102 at One Simulation Hour, Case 5

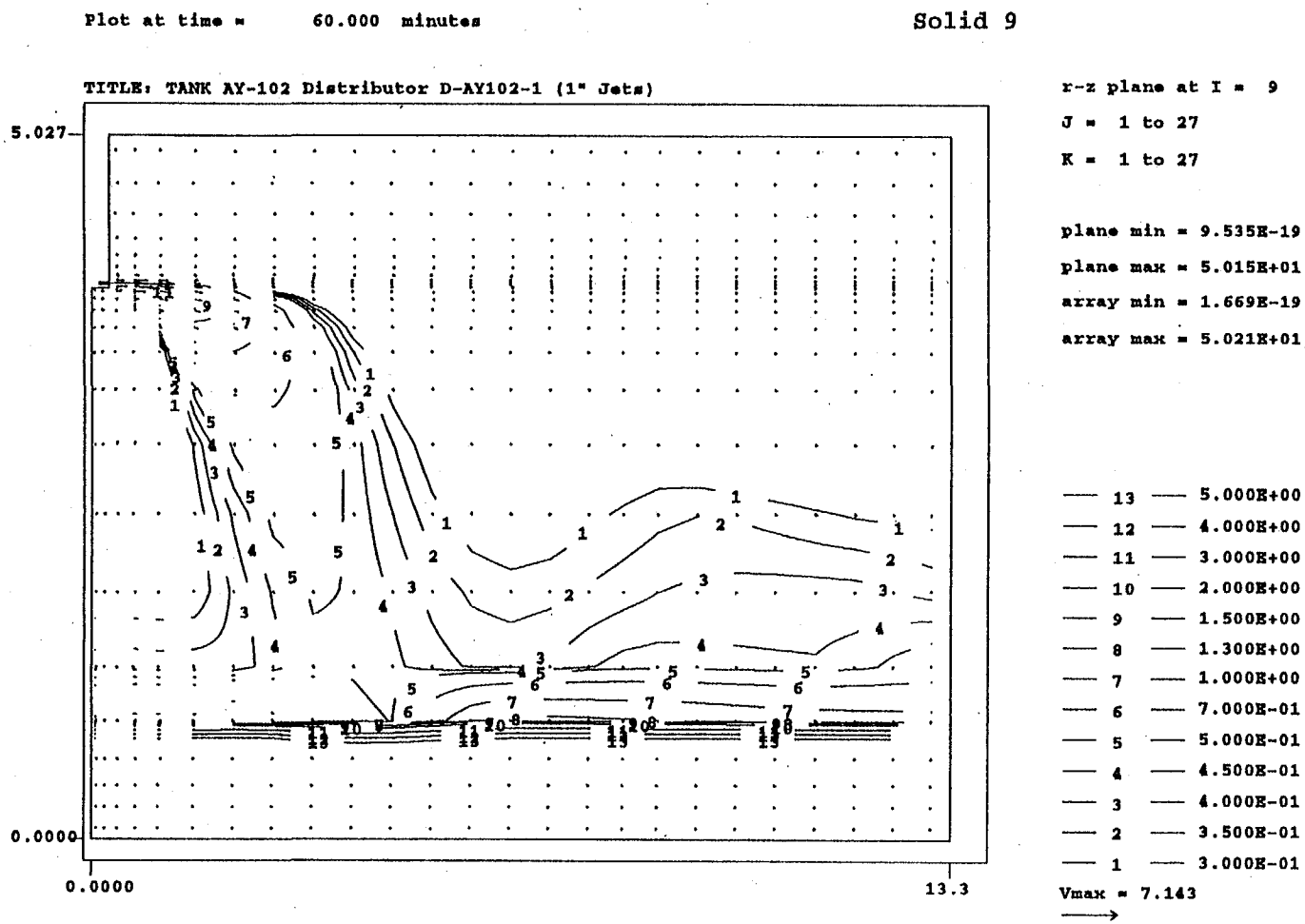

Figure 3.27. Predicted Vertical Distribution of Flow and Solid #9 Concentration on a Vertical Plane Containing One of the 1-in. Nozzles in Tank AY-102 at One Simulation Hour, Case 5

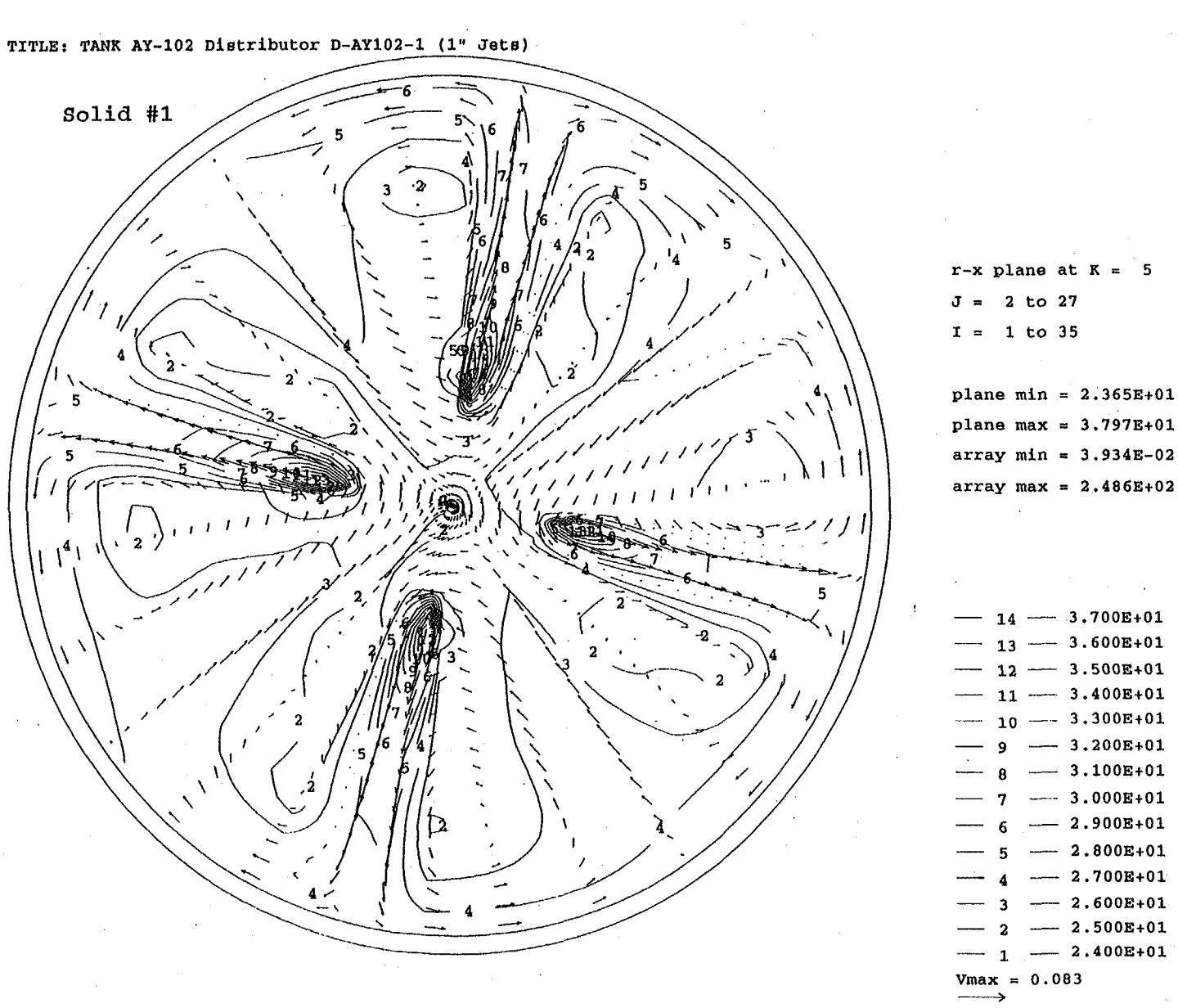

Figure 3.28. Predicted Horizontal Distributions of Flow and Solid #1 Concentration Just above the Original Sludge of Tank AY-102 at One Simulation Hour, Case 5

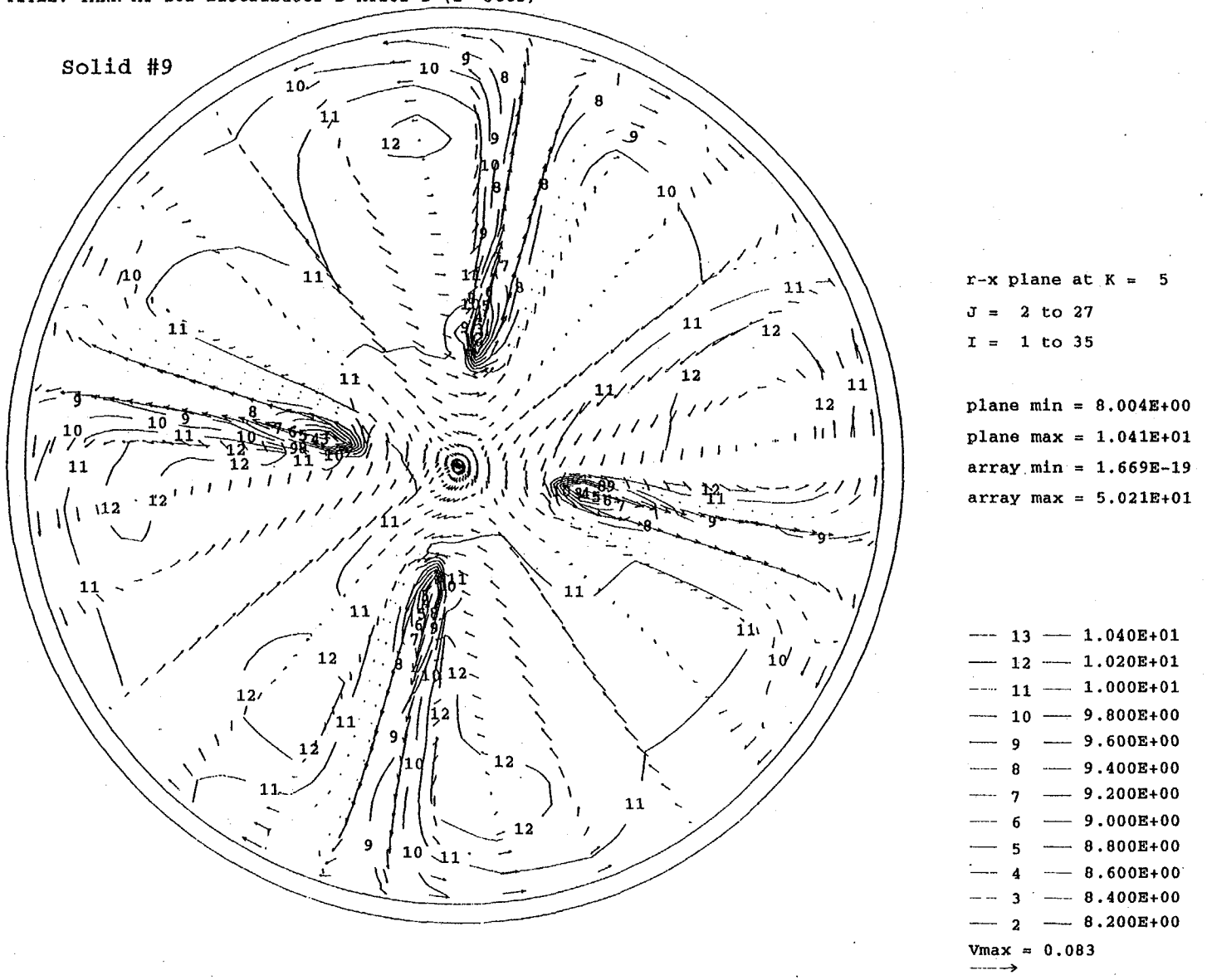

Figure 3.29. Predicted Horizontal Distributions of Flow and Solid #9 Concentration Just above the Original Sludge of Tank AY-102 at One Simulation Hour, Case 5

4.0 Summary and Conclusions

This study evaluated the C-106 slurry mixing and accumulation in Tank AY-102 using the TEMPEST computer code for the following five cases:

- Case 1: 3 wt% Slurry in 6.4-m AY-102 Waste. This case represents the 350 gpm-release of C-106 slurry with 3 wt% solids in AY-102 102 under Phase 2 initial operation (sludge and supernatant liquid thickness of 30 cm and 6.1 m, respectively)

- Case 2: 3 wt% Slurry in 4.3-m AY-102 Waste. This case represents the 350 gpm-release of C-106 slurry with 3 wt% solids in AY-102 under Phase 1 initial operation (sludge and supernatant liquid thickness of 30 cm and 4.0 m, respectively)

- Case 3: 30 wt% Slurry in 6.4-m AY-102 Waste. This case represents the 350 gpm-release of C-106 slurry with 30 wt% solids in AY-102 102 under Phase 2 Operation (sludge and supernatant liquid thickness of 30 cm and 6.1 m, respectively)

- Case 4: 30 wt% Slurry in 4.3-m AY-102 Waste. This case represents the 350 gpm-release of C-106 slurry with 30 wt% solids in AY-102 102 under Phase 1 Operation (sludge and supernatant liquid thickness of 30 cm and 4.0 m, respectively)

- Case 5: 30 wt% Slurry in 5.0-m AY-102 Waste. This case represents the 300 gpm-release of C-106 slurry with 30 wt% solids in AY-102 (sludge and supernatant liquid thickness of 45 cm and 4.5 m, respectively).

The model study indicates that the solid depth accumulated at the Enraf densitometer at riser 15S is within 5% of the average solids accumulation. Thus, the Enraf reading can be used to represent the total mass of transferred solids reasonably well.

The AY-102 model showed all five cases with the C-106 slurry jets descending toward the tank bottom because a heavier C-106 slurry is being injected into the lighter AY-102 supernatant liquid. Predicted solid concentrations for all five cases exhibit significant vertical variations. Case 2 exhibits the smallest vertical variation of solid concentrations above the solid setting layer; Solid #1 shows approximately 100% variation and Solid #9 shows about four orders of magnitude variation. Case 5 had the largest vertical solid concentration variation; Solid #1 varied about 200-fold and Solid #9 about 18 orders of magnitude.

For Cases 1 and 2, with only 3 wt% solids, C-106 slurry jets hit the farthest tank wall 2.3 m above the tank bottom. In Cases 3 and 5, though, with 30 wt% solids, the C-106 slurry jets descended much more rapidly, and the plume centers hit the tank bottom and slid along the surface of the original AY-102 sludge layer. Table 4.1 shows the predicted dilution of C-106 solids by the time the C-106 slurry hit the farthest tank wall.

Table 4.1. Predicted Reduction of C-106 Solids at the Farthest Tank Wall after 1 hr of Slurry Transfer

	Solids Loading at Injection (kg/m^3)	Solids Loading at Tank Wall (kg/m^3)	Reduction Factor
Case 1	30.34	2.222	13.7
Case 2	30.34	2.269	13.4
Case 3	368.6	21.845	16.9
Case 4	368.6	21.951	16.8
Case 5	366.2	27.451	13.3

Upon hitting the tank wall and bottom, the slurry jet slid along the surface of the original AY-102 sludge layer. The injection jets broke the slurry plume into four discrete fingers that hit the walls and swiveled back toward the center, producing fan-shaped isoconcentration contours.

Solid deposition patterns vary from case to case and solid to solid. For example, in Cases 1 and 2, the finer solids (Solids #1 and 4) accumulate along the tank wall, especially in the four places that the plumes hit, and the tank center accumulates the least solids. The coarser solids (Solid #9) accumulate least along the tank wall, except where the four plumes hit, and most around the tank center. In Cases 3, 4, and 5, with 30 wt% solids, the finer solids accumulate around the four areas the slurry jets hit and much less around the tank center. The coarser solids accumulate more in the area where the reflected slurry flow goes after it hits the tank wall. Much smaller amounts were deposited around the tank center in these cases. In Cases 3 through 5, there is still a significant density difference between the slurry sliding over the original AY-102 nonconvective layer and that near the waste surface, making it difficult for the diluted slurry to move upward and preventing much of the solids from being recirculated back to Tank C-106.

The horizontal distributions of solid concentrations are much more uniform than the vertical distributions in all five cases. This is clearly indicated by the additional layer produced by the deposited solids. Estimated accumulated depths immediately above the original AY-102 nonconvective layer are shown in Table 4.2 for all five cases; Case 2 has the largest accumulated depth variation. The table indicates relatively small variations of the accumulated depth; the ratio of the maximum accumulated depth to the average depth is within 24% for all five cases. The depth at riser 15S is expected to be within 5% of the average accumulated depth in all cases.

Table 4.2. Estimated Depth Variations of C-106 Solid Accumulation in Tank AY-102 after 1 hr of Slurry Transfer

	Ratio of Maximum to Average Depth	Ratio of Average Depth to Depth at Riser 15S	Ratio of Maximum Depth to Depth at Riser 15S
Case 1	1.14	0.970	1.11
Case 2	1.24	1.05	1.30
Case 3	1.09	0.963	1.05
Case 4	1.10	0.976	1.07
Case 5	1.07	0.955	1.02

5.0 References

Brandsma MG and DJ Divoky. 1976. *Development of Models for Prediction of Short-Term Fate of Dredged Material Discharged in the Estuarine Environment*, Tetra Tech. Inc., Pasadena California. Prepared for U.S. Army Engineer Waterways Experimentation Station, Vicksburg, Mississippi.

Brandsma MG and TC Sauer. 1983. "The OOC Model: Prediction of Short Term Fate of Drilling Mud in the Ocean. Part 1: Model Description." *Proceedings of the Mineral Management Service Workshop in an Evaluation of Effluent Dispersion and Fate Models for OCS Platforms.* February 7-10, 1983, Santa Barbara, California, pp. 58-84. .

Castaing BA. 1994. *101-AY, 102-AY, & 106-C Data Compendium.* WHC-SD-T1-578 Rev. 1, Westinghouse Hanford Company, Richland, Washington.

Carothers KG, SD Estey, NW Kirch, LA. Stauffer, and JW Bailey. 1998. *Tank 241-C-106 Waste Retrieval Sluicing System Process Control Plan.* HNF-SDF-WM-PCP-013 Rev. 0, Lockheed Martin Hanford Corporation, Richland, Washington.

Lumetta GJ, MJ Wagner, FV Hoopes, and RT Steele. 1996. *Washing and Caustic Leaching of Hanford Tank C-106 Sludge.* PNNL-11381, Pacific Northwest National Laboratory, Richland, Washington.

Mahoney LA and DS Trent. 1995. *Correlation Models for Waste Tank Sludge and Slurries.* PNL-10695, Pacific Northwest National Laboratory, Richland, Washington.

Onishi Y. 1994. "Contaminant Transport Models in Surface Waters." *Computer Modeling of Free Surface and Pressurized Flows,* MH Chaudrey and LW Mays, eds. NATO ASI Series E, Applied Sciences, Klumer Academic Publisher, Dordrecht, The Netherlands, Vol. 274, Chapter 11, pp. 313-341.

Onishi Y, HC Reid, DS Trent, and JD Hudson. 1996a. "Tank Waste Modeling with Coupled Chemical and Hydrothermal Dynamics." *Proceedings of 1996 National Heat Transfer Conference.* American Nuclear Society, Houston, pp. 262-269.

Onishi Y, R Shekarriz, KP Recknagle, PA Smith, J Liu, YL Chen, DR Rector, and JD Hudson. 1996b. *Tank SY-102 Waste Retrieval Assessment: Rheological Measurements and Pump Jet Mixing Simulation.* PNNL-11352, Pacific Northwest National Laboratory, Richland, Washington.

Onishi Y and KP Recknagle. 1997. *Tank AZ-101 Criticality Assessment Resulting from Pump Jet Mixing: Sludge Mixing Simulations.* PNNL-11486, Pacific Northwest National Laboratory, Richland, Washington.

Onishi Y and KP Recknagle. 1998. *Performance Evaluation of Rotating Pump Jet Mixing of radioactive Wastes in Hanford Tanks 241-AP-102 and 241-AP-104,* PNNL-11920, Pacific Northwest National Laboratory, Richland, Washington.

Onishi Y and DS Trent. 1998. *TEMPEST Code Modifications and Testing for Erosion-Resisting Sludge Simulations.* PNNL-11787, Pacific Northwest National Laboratory, Richland, Washington.

Perry RH and CH Chilton. 1973. *Chemical Engineering Handbook.* McGraw-Hill, New York.

Rodi W. 1984. *Turbulence Models and Their Application in Hydraulics.* Institute of Hydromechanics, University of Karlsruh, Germany.

Runchal. 1983. *The Proceedings of the Mineral Management Service Workshop in an Evaluation of Effluent Dispersion and Fate Models for OCS Platforms.* Santa Barbara, California.

Terrones G and LL Eyler. 1993. *Computer Modeling of ORNL Storage Tank Sludge Mobilization and Mixing.* PNL-8855, Pacific Northwest Laboratory, Richland, Washington.

Trent DS and TE Michener. 1993. *Numerical Simulation of Jet Mixing Concepts in Tank 241-SY-101.* PNL-8559, Pacific Northwest Laboratory, Richland, Washington.

Vanoni VA, ed. 1975. *Sedimentation Engineering.* ASCE Manuals and Reports on Engineering Practice, ASCE, New York.

Whyatt GA, RJ Serne, SV Mattigold, Y Onishi, MR Powell, JH Westik Jr., LM Liljegren, GR Golcar, KP Recknagle, PM Doctor, VG Zhirnov, and J Dixon. 1996. *Potential for Criticality in Hanford Tanks Resulting from Retrieval of Tank Waste.* PNNL-11304, Pacific Northwest National Laboratory, Richland, Washington.

Distribution

No. of Copies

Offsite

2 DOE Office of Scientific and Technical Information

D. M. Ogden
12122 N. Guinevere Dr.
Spokane, WA 99211

Onsite

2 DOE Richland Operations Office

W. Abdul	S7-53
C. A. Groendyke	S7-54

18 PHMC Team

K. J. Anderson	S5-04
J. W. Bailey	S2-48
W. B. Barton	R2-11
R. E. Bauer	S7-14
K. G. Carothers	R2-11
C. E. Hanson	G1-54
G. N. Hanson	S5-07
G. D. Johnson	S7-14
N. W. Kirch	R2-11
J. W. Lentsch (5)	S2-48
D. A. Reynolds	R2-11
K Sathyanayarana	H0-34
L. A. Stauffer	R2-11
R. G. Stickney	R1-49

24 Pacific Northwest National Laboratory

J. M. Bates	K7-15
S. Q. Bennett	K7-90
J. W. Brothers	K5-22
W. L. Kuhn	K7-15
P. A. Meyer	K7-15
Y. Onishi (7)	K7-15
K. P. Recknagle (3)	K7-15
C. W. Stewart (3)	K7-15
W. C. Weimer	P7-27
Information Release (5)	K1-06